

Original paper

# Mineralogy and evolution of the epithermal mineralization in the Rudno nad Hronom–Brehy ore deposit, Štiavnické vrchy Mts. (Slovakia)

Jozef VLASÁČ<sup>1\*</sup>, Tomáš MIKUŠ<sup>1</sup>, Juraj MAJZLAN<sup>2</sup>, Martin ŠTEVKO<sup>3,4</sup>, Adrián BIRÓN<sup>1</sup>,  
Marek SZCZERBA<sup>5</sup>, Rastislav MILOVSKÝ<sup>1</sup>, Peter ŽITŇAN<sup>6</sup>

<sup>1</sup> Earth Science Institute v.v.i., Slovak Academy of Sciences, Ďumbierska 1, 97411 Banská Bystrica, Slovakia; vlasac@savbb.sk

<sup>2</sup> Institute of Geosciences, Friedrich-Schiller University, Burgweg 11, 07749 Jena, Germany

<sup>3</sup> Earth Science Institute v.v.i., Slovak Academy of Sciences, Dúbravská cesta 9, 84005 Bratislava, Slovakia

<sup>4</sup> Department of Mineralogy and Petrology, National Museum, Cirkusová 1740, Prague 9, 19300 Horní Počernice, Czech Republic

<sup>5</sup> Institute of Geological Sciences, Polish Academy of Sciences, Sanecka 1, 31-002 Krakow, Poland

<sup>6</sup> Department of Geology and Palaeontology, Faculty of Natural Sciences, Comenius University in Bratislava, Ilkovičová 6, 84215 Bratislava, Slovakia

\*Corresponding author



The Rudno nad Hronom–Brehy ore deposit in Slovakia represents an important locality of epithermal precious metal mineralization in the Central Slovak Volcanic Field. The main ore structures in the area are Anna, Goldschram, Filip, Johan de Deo and Priečna veins. In this work, we present mineralogical, paragenetic and geochemical aspects of the ore mineralization, hydrothermal alteration patterns, fluid inclusions, isotopic composition of sulfur ( $\delta^{34}\text{S}$ ) and K–Ar age of ore mineralization. Four mineralization stages were recognized, the third one being split into two substages. (1) Pyrite stage with quartz, K-feldspar, arsenopyrite and pyrite. (2) Base-metal stage with sphalerite, galena, chalcopyrite, Au–Ag alloys and famatinite. (3a) Early Ag stage with tetrahedrite-(Zn), tetrahedrite-(Fe), argentotetrahedrite-(Zn), tetrahedrite-(Cd), argentotetrahedrite-(Cd) and greenockite. (3b) Late Ag stage with pyrargyrite, polybasite, pearceite, cupropolybasite, cupropearceite, acanthite and galena. (4) Late Ag–Cu stage with bornite, stromeyerite, mckinstryite, chalcocite, digenite, covellite and uytenbogaardtite. Veins are rich in silver with an average Ag:Cu ratio of 85:1; in some parts of the veins, Ag content reaches up to 1950 ppm and Au up to 42.7 ppm. The neutral to alkaline style of hydrothermal alteration is represented by K-feldspar, quartz, carbonates, smectite, interstratified illite/smectite, and chlorite (clinochlore, chamosite). This assemblage indicates a low sulfidation origin of the mineralization formed at 177–224 °C. The  $\delta^{34}\text{S}$  values from the base-metal stage varies from +2.8 to +3.5 ‰ for chalcopyrite from the northern part of the Priečna vein, from +1.9 to +2.6 ‰ for galena, from +4.9 to +5.2 ‰ CDT for pyrite from the Anna vein. These values indicate a relatively homogeneous sulfur source, most likely related to an igneous or mixed igneous and host-rock source. Fluid inclusions in quartz associated with the base-metal stage have low salinity (1.1–1.6 wt. % NaCl eq.) and homogenization temperatures of 176–250 °C. The available data suggest that the base-metal stage was accompanied by cooling and dilution owing to a meteoric fluid. The temperature estimated from the tetrahedrite thermometer of the early Ag stage is ~170–205 °C. According to the paragenetic relationship and mineral stability, the deposition temperatures in the late Ag stage did not exceed 160 °C. The late Ag–Cu stage formed at temperatures of <93 °C. The results of K–Ar radiometric dating from the hydrothermal alteration returned an average age of  $12.5 \pm 0.3$  Ma. The studied mineralization is possibly related to the initial stage of resurgent horst tectonic activity and rhyolite volcanism of the fifth stage of Štiavnica stratovolcano formation.

**Keywords:** mineralogy, geochemistry, epithermal mineralization, Štiavnica stratovolcano, neovolcanites

Received: 10 March 2023; accepted: 29 September 2023; handling editor: J. Zachariáš

The online version of this article (doi: 10.3190/jgeosci.380) contains electronic supplementary material.

## 1. Introduction

The Au–Ag epithermal deposit at Rudno nad Hronom and Brehy is part of the Nová Baňa–Rudno–Pukanec ore district. It is located in the SW part of the Štiavnica stratovolcano that belongs to the Neogene–Quaternary

Central Slovak Volcanic Field (CSVF). The Štiavnica stratovolcano hosts numerous epithermal, porphyry and skarn mineralizations, many of them intensively studied in the past decades (Lexa et al. 1999; Bahna and Chovan 2001; Koděra et al. 2005, 2010, 2014; Bakoš et al. 2010; Berkh et al. 2014; Majzlan et al. 2016, 2018; Kozák et al.

2017; Kubač et al. 2018). The Banská Štiavnica–Hodruša ore deposit comprise of many epithermal vein systems that contain precious and base-metal mineralization exploited from the Middle Ages to the present. During the last four centuries, the Banská Štiavnica–Hodruša deposit yielded more than 80 tons of Au and 4000 tons of Ag (Lexa et al. 1999).

The formation of the various deposits in the Štiavnica stratovolcano is related to long-lasting volcanic activity from Middle Miocene to the Pleistocene. The maximum of the volcanic activity occurred between 15.0 and 11.4 Ma (Chernyshev et al. 2013). The Štiavnica stratovolcano is the largest one among the seven different volcanic centres within the CSFV. The stratovolcano formed during several stages (Konečný 1971; Konečný and Lexa 2000) accompanied by distinct types of ore mineralizations (Lexa et al. 1999).

## 2. Geological setting

### 2.1. Evolution of the Štiavnica stratovolcano and ore mineralizations

Prior to the onset of volcanic activity, the pre-Neogene basement in the area of the today's stratovolcano consisted of Carboniferous–Permian rocks. They include Carboniferous sandstones, claystones with graphitic admixture (Hronic nappe – Nižná Boca fm.), Permian volcano–sedimentary complex (basalts with tuffitic claystones and sandstones, Hronic nappe – Malužiná fm.) and Triassic sedimentary complexes (limestones and micaceous sandstones of Krížna nappe; Brly et al. 1977).

The first stage of the stratovolcano evolution (lower stratovolcano structure or pre-caldera stage) represents the onset of volcanic activity between 15.0–13.6 Ma (Chernyshev et al. 2013). This stage is characterised by the explosive and effusive activity of pyroxene, hornblende–pyroxene, biotite–hornblende–pyroxene andesites. It created an extensive stratovolcano approximately 50 km in diameter and estimated height of up to 4 km (Konečný et al. 1998a). In the southern part of the stratovolcano, diorite porphyry intruded between the lower stratovolcano structure and the pre-Neogene basement. This intrusion is responsible for the formation of porphyry gold mineralization in Beluj with uneconomic resources estimated at 58.4 Mt ore with 0.3 ppm Au (Bakoš et al. 2010; Kozák et al. 2017). A large diorite intrusion in the centre of the stratovolcano gave rise to the high-sulfidation mineralization in the Šobov hydrothermal system. The yet uneroded roots of this mineralization consist mainly of metasomatic quartzite (Lexa et al. 1999).

The second stage (intrusive or early caldera stage) is characterised by a long-lasting break in the volcanic activity and uplift of the central zone of the stratovolcano. Extensive denudation lowered the total height of the stratovolcano from 4 km to a maximum of 1 km (Chernyshev et al. 2013). Several intrusive complexes were emplaced during this stage. In the initial phase, the granodiorite subvolcanic pluton intruded beneath the andesites of the first stage and formed a large, so-called “bell jar” pluton. In this phase, Fe-skarn in Vyhne was formed between the contact of granodiorite and Mesozoic sedimentary rocks of the basement. There is also stockwork/disseminated base metal mineralization spatially and genetically related to the apical zones of granodiorite pluton (Koděra et al. 2004). Initial subsidence was accompanied by the emplacement of quartz-diorite porphyry sills following subhorizontal faults (low-angle normal fault shear zone). These intrusive complexes are bound to well-developed multi-stage intermediate-sulfidation Au–Ag–base metal mineralization developed at the Rozália mine. Veins developed on low-angle normal faults (LANF) were systematically studied since the 1990's and are currently mined for gold and silver (Koděra et al. 2005; Kubač et al. 2018). Finally, in the second phase, intrusive complexes of granodiorite/quartz-diorite porphyry clusters and stocks intruded around the granodiorite pluton. In the apical and marginal sides of these intrusions, Cu–Au porphyry/skarn mineralization has formed (Zlatno deposit). The mineralized zone is represented by accumulations of chalcopyrite in exo- and endo-skarns in sedimentary Mesozoic blocks of the basement enclosed in the intrusive bodies. The apical parts of the intrusions show typical porphyry alteration patterns with disseminated Cu–Au ores (Lexa et al. 1999; Koděra et al. 2010).

In the third stage (caldera stage), the intensive subsidence of the caldera followed the volcanic activity of amphibole–biotite–plagioclase andesites to dacites. They formed mainly extrusive domes, dome flows, pyroclastic flow breccias, ignimbrites and epiclastic volcanic breccias. This stage is devoid of any significant ore mineralization (Rottier et al. 2020).

The fourth stage (post-caldera stage) is characterised by the effusive activity of orthopyroxene–plagioclase andesite lava flows, ignimbrites, epiclastic breccias and the final period of the caldera subsidence (Rottier et al. 2020). Volcanic rocks of the third and fourth stage were almost completely eroded.

The fifth stage is marked by an intensive tectonic activity that is responsible for the current morphological form of the Štiavnica stratovolcano. This tectonic activity segmented the existing stratovolcano into resurgent horst and created conditions for the evolution of base metal and precious-metal epithermal systems in the

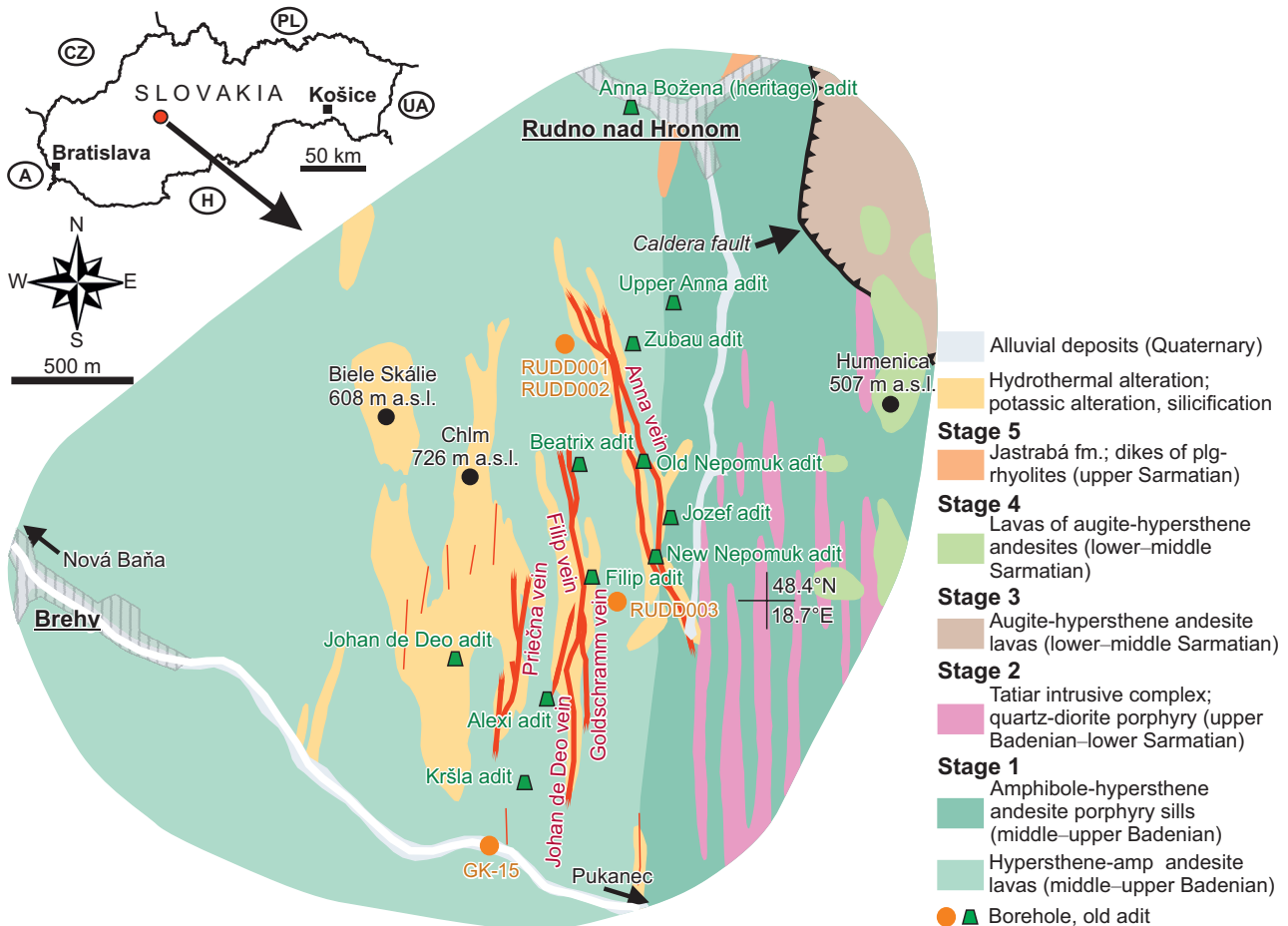


Fig. 1 Geological map of the study area with marked old mine workings, boreholes and vein structures (after Konečný et al. 1998b).

caldera. The mineralization mainly occupies marginal faults of the resurgent horst, associated in space and time with the emplacement of rhyolites of the Jastrabá formation. Two types of horst uplift related veins are recognised. Sulfide-rich base-metal (“Štiavnica type”) in the central part of the stratovolcano with Ag: Au ratio from 10:1 to 20:1 and silver±base metal (“Hodruša type”) in the western part of the stratovolcano with Ag: Au ratio up to 100:1 (Lexa et al. 1999). Their age was determined as 12.2–11.4 Ma by radiometric methods (Lexa et al. 1999; Chernyshev et al. 2013; Rottier et al. 2020) or as  $12.3 \pm 1.0$  Ma in volcanic glass to  $12.1 \pm 1.1$  Ma in biotite by fission-track counting (Repčok 1982).

Despite of significant commercial and scientific interest in these deposits, the smaller ones, even though exploited historically, were not given sufficient attention. An example thereof is the precious-metal mineralization in Rudno nad Hronom–Brehy. This study aims to clarify mineralogy, geochemistry and the metallogenetic aspects of this ore mineralization and thus bring new data on the development and evolution of the ore mineralization of the entire Štiavnica stratovolcano.

## 2.2. Regional geological situation and historical background

The epithermal deposit at Rudno nad Hronom–Brehy area is located at the SW flank of the Štiavnica stratovolcano ( $48.39837^\circ\text{N}$ ,  $18.68571^\circ\text{E}$ ), in the southern and eastern slope of Chlm hill extrusive complex over an area of  $1.5 \times 3$  km<sup>2</sup> (Fig. 1). The mineralization is hosted by five large veins related to a local horst, namely Anna, Filip, Goldschram, Johan de Deo and Priečna vein. The veins have mostly N–S to NNW–SSE strike and are hosted by the first-stage andesitic complex of the stratovolcano. In the western part of the ore field, there are numerous swarms of granodiorite/quartz-diorite porphyry dikes which belong to the second stage of stratovolcano evolution. In the northern part of the deposit, a dike of rhyolite (Jastrabá formation) of the fifth stage is emplaced between the marginal contact of the Chlm hill extrusive complex and the sills of andesite porphyry which belongs to the first stage of the stratovolcano evolution. Štohl et al. (1993) assumed a genetic link between the mineralization in Rudno nad Hronom–Brehy area and the fifth-stage rhyolite volcanism. This statement is supported by the

fact that some of the ore veins occupy the same tectonic structures as the rhyolites.

The ore veins are accompanied by extensive hydrothermal alteration. Proximal zones are characterised by abundant K-feldspar with quartz, pyrite, and illite/smectite assemblages surrounded by argillitic alterations (illite/smectite, chlorite, pyrite). The distal parts experienced propylitization with chlorite, epidote, pyrite, and quartz as typical minerals (Smolka et al. 1988).

The **Anna vein** is the easternmost mineralized zone located on the eastern slope of the Chlm hill with a length of 1.5 km and dip 50–70° to W (Lexa and Smolka 2002). Mineralized zones are developed on the contact of the Chlm intrusive andesitic complex and older first-stage andesite porphyry. Historical data show that the subject of exploitation was only a 200 m long section where the overlying (“golden”) and underlying (“silver”) veins intersected and formed ore pillars up to 42 m thick. The first written documents date back to 1702 when it was remarked that the mine is “ancient”. The sulfide concentrates from the richest zones contained 470–780 g/t Au+Ag (Bergfest 1953).

The **Johan de Deo, Goldschram and Filip veins** are the central vein systems in the investigated ore field with a total length of 1.5 km. The veins are up to 1 m thick. The Johan de Deo and Filip veins dip steeply (65–90°) to W, the Goldschram vein dips in the central part and in the deeper portions steeply to E. In 1921, the production was 0.5 kg of gold and 34 kg of silver (Bergfest 1953).

The least explored **Priečna vein** is located 250 m to the west of the Johan de Deo and Filip veins, with a total length of 1.1 km (Lexa and Smolka 2002). There are no further data on this vein.

### 3. Samples and analytical methods

Anna vein samples were collected from the dumps of old adits. Samples from the central part of the Johan de Deo, and Filip and Priečna veins were collected from the mineralized zones accessible *via* the lower Johan de Deo adit. Samples for the study of the hydrothermal alterations were obtained from the exploration drill cores.

Textural and compositional relationships were further investigated with an electron microprobe (EMP) JEOL JXA 8530FE (at Earth Science Institute of Slovak Academy of Sciences in Banská Bystrica). Back-scattered electron (BSE) images were acquired to document the textures. Reconnaissance semi-quantitative chemical analyses of oxide, carbonate and silicate minerals were acquired with energy-dispersive X-ray spectrometry (EDX). Selected minerals were quantitatively analysed using wavelength-dispersive spectrometry (WDX). The beam size was 1–10 µm, with an accelerating voltage of

20 kV and a probe current of 15 nA. The WDX spectrometers were used to measure the elements and X-ray lines of Au (L $\alpha$ ), Ag (L $\alpha$ ), Cu(K $\alpha$ ), Zn (K $\alpha$ ), Pb (M $\alpha$ ), Fe (K $\alpha$ ), As (L $\beta$ ), Sb (L $\alpha$ ), Cd(L $\alpha$ ), Se (L $\alpha$ ), Te (L $\alpha$ ), Bi (L $\alpha$ ), Hg (M $\alpha$ ) and S (K $\alpha$ ). The counting times for all elements were 20 s at the peak and 10 s for each background. Raw intensities were converted to the concentrations of elements using automatic ZAF matrix-correction software. Natural and synthetic standards included Au for Au, Ag<sub>2</sub>S for Ag, CdTe for Cd and Te, CuFeS<sub>2</sub> for Cu, ZnS for Zn, PbS for Pb, FeS<sub>2</sub> for Fe and S, GaAs for As, Sb<sub>2</sub>S<sub>3</sub> for Sb, Bi<sub>2</sub>Se<sub>3</sub> for Se and Bi and HgS for Hg.

Bulk samples were analysed for Au by atomic absorption spectroscopy (AAS) and the remaining elements by inductively-coupled plasma atomic emission spectroscopy (ICP-AES) in the laboratories of ALS CHEMEX in Rosia Montana, Romania. Analyses of drill core samples and those collected on the surface or in the adits were kindly provided by the exploration company Prospech Ltd. The detection limit for Au (AAS, methodology code Au-AA25) is 0.01 ppm. One quarter of the sample was subjected to ICP-AES analysis of other elements (methodology code ME-ICP61). Detection limits in ppm for this method are: Ag 0.5, Al 100, As 5, Ba 10, Bi 2, Ca 100, Cd 0.5, Cu 1, Fe 100, K 100, Mg 100, Mn 5, Mo 1, Na 100, Pb 2, S 100, Sb 5, Se 10, Sn 10, Sr 1, Te 10, Ti 100, V 1, Zn 2. For over-limited Ag content in the sampling method, Ag-OG62 and Ag-GRA21 were used.

Stable isotopes of sulfur ( $\delta^{34}\text{S}$ ) were measured with an isotope-ratio mass spectrometer (IRMS) MAT 253 coupled to an elemental analyser Flash2000Ht Plus Via a continuous-flow interface ConFlo IV (Thermo Scientific; at Earth Science Institute of Slovak Academy of Sciences in Banská Bystrica). Weighed samples (170–185 µg) were mixed with about the same amount of V<sub>2</sub>O<sub>5</sub> and wrapped into tin capsules. Afterwards, samples were combusted with oxygen in a quartz tube filled with WO<sub>3</sub> and electrolytic copper at 1000 °C. The obtained SO<sub>2</sub> gas was purified on a packed GC-column (5 Å mol sieve at 90 °C) following into the IRMS. Analytical data were calibrated with the international standards IAEA-S2 and IAEA-S3 ( $\delta^{34}\text{S} = +22.7$  and  $-32.3\%$  CDT).

Double side polished sections with thickness of ~200 µm were prepared for the microthermometry study. Petrographic relationship between the fluid inclusion and mineral phases was determined by transmitted-light microscopy. Attention was paid to the distinction between primary and secondary fluid inclusions, using the criteria outlined in Roedder (1984). Fluid inclusions were subjected to cooling or heating in a Linkam THM-600 stage attached to the microscope (at Earth Science Institute of Slovak Academy of Sciences in Banská Bystrica). Triple points of natural inclusions of liquid CO<sub>2</sub> (–56.6 °C) and sulfur (119.2 °C) were used to calibrate the equipment.

Due to limited fluid inclusion size, eutectic temperatures were not observed. The accuracy of measurement is estimated at  $\pm 0.2^\circ\text{C}$  for temperatures ranging from  $-50^\circ\text{C}$  to  $0^\circ\text{C}$  and  $\pm 2^\circ\text{C}$  for temperatures ranging around  $350^\circ\text{C}$ . The basic parameters of fluid inclusions were calculated using computer software AqSo–NaCl (Bakker 2018), which implements the equations of Driesner and Heinrich (2007). The salinity of the fluid was estimated by observing the melting temperature of the last ice crystal upon rewarming using the equations from Bodnar (1993).

Powder X-ray diffraction (PXRD) was used to identify the minerals in hydrothermally altered rocks. Both bulk samples and clay fractions were analysed ( $<0.2$  and  $<2$   $\mu\text{m}$ ). The method described by Šucha et al. (1991) for separation of clay minerals was used. Preparation of whole-rock specimens for quantitative PXRD proceeded according to method developed by Środoń et al. (2001) and Eberl (2003). To achieve randomly oriented specimens, the method of spray drying was applied (Spray Drying Kit developed in The James Hutton Institute, Aberdeen, Scotland; Hillier 1999).

The PXRD analyses were performed on a Bruker D8 Advance diffractometer (at Earth Science Institute of Slovak Academy of Sciences in Banská Bystrica) using CuK $\alpha$  radiation generated at 40 kV and 40 mA, Beta-filter and position sensitive detector SSD160 operating in 1D mode. The beam was collimated with a slit assembly  $0.3^\circ$ – $6$  mm-PSD  $0.4984^\circ$ , primary and secondary Soller slits  $2.5^\circ$ . Analyses were performed as follows: step:  $0.01948^\circ 2\Theta$ , time/step: 0.8 s, interval  $2$ – $50^\circ 2\Theta$  (oriented samples) and time/step: 2 s and interval  $3$ – $70^\circ 2\Theta$  (disoriented samples). Oriented mounts were analysed air-dried and upon saturation with ethylene glycol (at  $60^\circ\text{C}$  for 8 hours). Data were processed with the software DIFFRAC.EVA (Bruker AXS 2010) and PDF2/2010 database. Identification of clay minerals was conducted mainly according to Moore and Reynolds (1997). The identification of illite-smectite type mixed-layer minerals and the quantification of the smectite component (expandability) were carried out by the method of the position of the basal reflexes after saturation with ethylene glycol of the  $<2$   $\mu\text{m}$  and  $<0.2$   $\mu\text{m}$  fractions (Reynolds 1980; Środoń 1981; Dudek and Środoń 1996). For quantitative PXRD phase analysis of samples the RockJock software was employed (Środoń et al. 2001; Eberl 2003). A geothermometer calibrated on the basis of smectite-to-illite conversion in sedimentary (diagenetic) environment (Šucha et al. 1993) was used to estimate formation temperatures of mineralization.

Selected samples were dated by the K–Ar method (at the Polish Academy of Sciences, Institute of Geological Sciences, Krakow, Poland). Three portions of each sample were weighed, the first two for potassium and the third one for argon measurement. The potassium contents

were measured using Sherwood Model 420 flame photometer. Radiogenic argon measurements were performed on Nu Instruments Noblesse multi-collector noble-gas spectrometer (NG039). The tantalum foil-wrapped portions were loaded into a titanium holder, which is a part of the preparatory line. The aliquots were subsequently evacuated to approximately  $10^{-10}$  mbar pressure. Each sample was melted by a defocused 972 nm infrared laser. CuO added to the samples enhanced the oxidation of organic matter during this step. Pure  $^{38}\text{Ar}$ , used as the spike, was introduced to the extraction line directly prior to the sample extraction, using a calibrated pipette.

Titanium sublimation getter was the first cleaning level of gases extracted from the samples. The final purification of argon was carried out in an isolated section of the line by a getter pump (Z-100, SAES Getters, previously baked overnight to remove excess argon). The amounts of gases poured into the spectrometer were optimised to keep  $^{40}\text{Ar}$  at the level below 0.15 V because, for higher pressures, fractionation on the Nier ion source can occur (Kellett and Joyce 2014). Gas aliquot released from the sample was measured two times by opening and closing valves of the line in a certain sequence. The same sample was melted for the second time, using the same procedure of measurements but with higher laser power.

The amount of the original aliquot of the  $^{38}\text{Ar}$  spike was determined by measuring the international standard GL-O (Odin 1982). This standard is measured at least four times with every batch of ten samples. Daily, the  $^{40}\text{Ar}/^{36}\text{Ar}$  and  $^{40}\text{Ar}/^{38}\text{Ar}$  ratios are measured for air sample aliquots delivered from a calibrated air pipette. Based on these results,  $^{40}\text{Ar}/^{36}\text{Ar}$  and  $^{40}\text{Ar}/^{38}\text{Ar}$  ratios were corrected for instrument mass fractionation and detector efficiencies assuming atmospheric ratios of ( $^{40}\text{Ar}/^{36}\text{Ar}$ )<sub>air</sub> = 298.57 and ( $^{40}\text{Ar}/^{38}\text{Ar}$ )<sub>air</sub> = 1583.5 (Lee et al. 2006). Age errors were calculated from the law of error propagation, taking into account uncertainties of spectrometric measurement of argon isotopes, weighting, potassium measurements, normalisation of the amount of  $^{38}\text{Ar}$  in spike based on dating of GL-O standard and assessment of  $^{40}\text{Ar}/^{36}\text{Ar}$  and  $^{40}\text{Ar}/^{38}\text{Ar}$  ratios, measured every day for air aliquots. Potassium measurements were performed on the two portions of HF dissolved (with 3–4 drops of  $\text{H}_2\text{SO}_4$ ) samples in order to increase the precision of K content estimation. After the reaction, HF was evaporated, and the procedure was repeated. Finally, the sample was dissolved in diluted HCl and proceeded to photometric measurements. The final amount of potassium in each sample was calculated as the average results received for the two aliquots. For several samples a few measurements were performed in order to improve precision. In these cases final ages were calculated as averages and error was calculated from uncertainties of single measurements via error propagation.

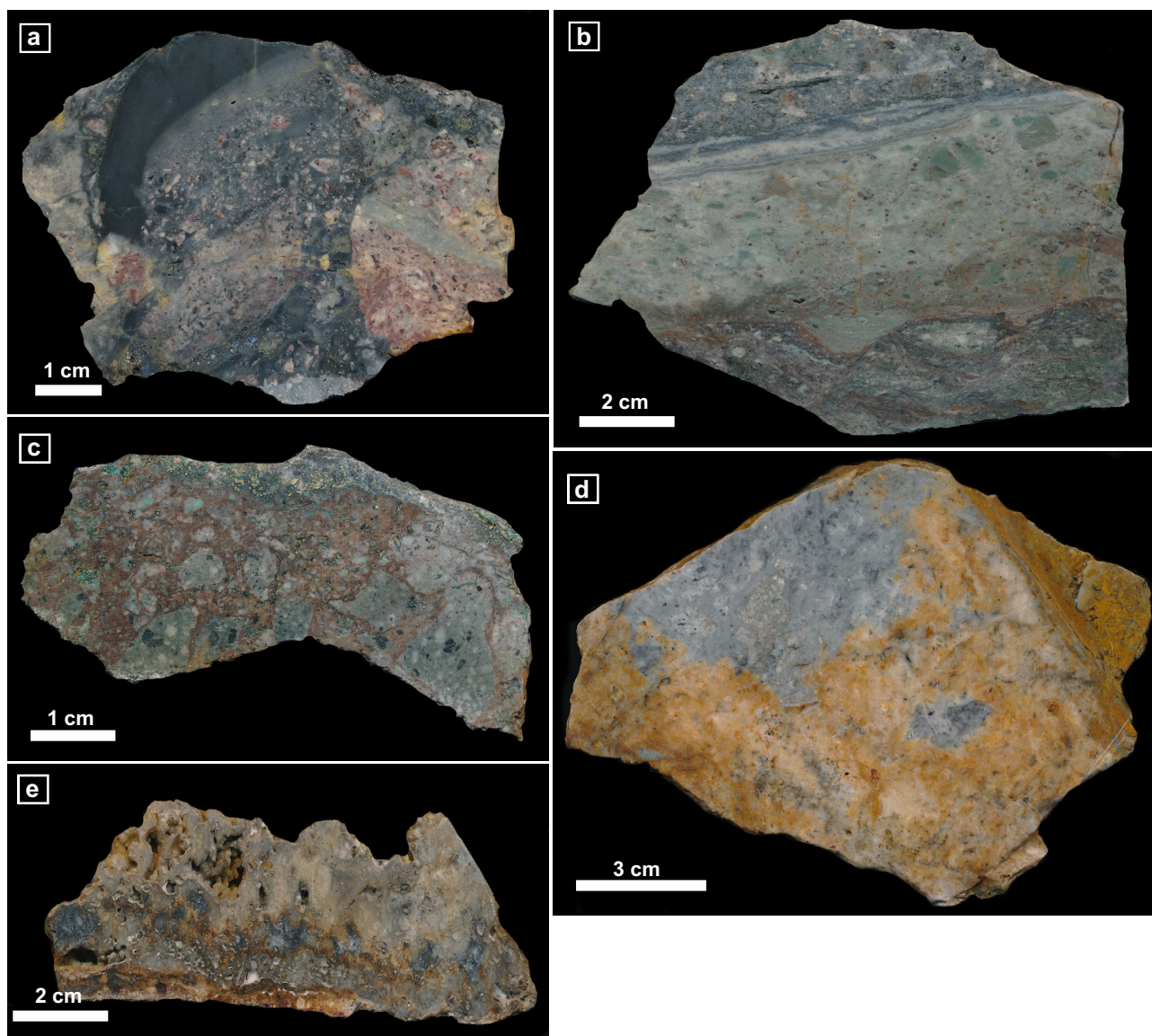


**Fig. 2a** – Hydrothermal breccia from the Zubau adit (Anna vein) composed of K-feldspar, quartz and base-metal mineralization. **b** – Intensively silicified breccia from the southern part of the Priečna vein with high-grade Au–Ag mineralization. **c** – Silicified breccia from the northern part of the Priečna vein with rich chalcopyrite and Au–Ag mineralization. **d** – Quartz to chalcedony with impregnation of ore mineralization. **e** – Chalcedony impregnated by Au–Ag mineralization from the Kršľa adit (Johan de Deo vein).

Tables containing the complete data set of collected WDS (supplementary material S1) and bulk chemistry analyses of ore (supplementary material S2) are included in supplementary files for this paper.

## 4. Results

### 4.1. Ore textures

The most common textural forms in the studied samples are breccia textures. Polyphase mineralization of the Anna vein is represented by quartz and K-feldspar fragments cemented with fine-grained quartz and min-

erals of pyrite and base-metal stage (Fig. 2a). The size of the fragments is variable, ranging from a few mm to a few cm. In the Priečna vein, intensively silicified breccia is composed of fine-grained quartz, K-feldspar and chalcedony fragments with disseminated Au–Ag and base metal mineralization in the matrix (Fig. 2b). Pyrite, base-metal, early and late Ag, late Ag–Cu stages were identified in this ore type. According to the textural observation, ore textures from the Priečna vein can be divided into base-metal rich in the northern part represented by the macroscopic chalcopyrite and Ag sulfide/sulfosalts rich in the southern part of the vein represented by the macroscopic polybasite and pyrargyrite.

Euhedral polybasite and pyrargyrite of the late Ag stage crystals commonly occur in the cavities from the southern part of the Priečna vein. In some cases, quartz fragments cemented by quartz K-feldspar matrix are cut by veinlets (thickness up to 2 cm) of colloform chalcocite and galena (late Ag stage).

In the northern part of the Priečna vein, breccia consists of irregular fragments of altered andesite, cemented by a fine-grained quartz and K-feldspar matrix (Fig. 2c). In this part of the vein, disseminated ore mineralization is formed by rich chalcopyrite (base-metal stage rich) ore in the form of irregular clusters several mm in the matrix of breccia.

In the southern part of the Johan de Deo vein, porous to massive chalcocite contains abundant disseminated ore minerals (Fig. 2e) of base-metal, early Ag and late Ag stage. Similar type of ore was observed in the Goldschram-Filip vein intersection (Fig. 2d); however, minerals of late Ag-Cu stage were not identified there.

#### 4.2. Ore mineralogy and chemistry

Ore mineralization is closely related to quartz and K-feldspar alteration around ore veins. It is generally concentrated in the matrix of mineralized hydrothermal breccias. In some cases (Johan de Deo vein), the ore mineralization is dispersed in porous chalcocite. The mineral content of the assemblages at Rudno nad Hronom-Brehy varies from vein to vein or can vary even within a single vein (see below). In the Anna vein, only base-metal sulfides were found and the minerals of the Ag and Ag-Cu stages missing. Ore mineralization of the deposit was divided into four stages, the third one having two substages: (1) pyrite stage, (2) base-metal stage, (3a) early Ag stage, (3b) late Ag stage and (4) late Ag-Cu stage. The chemical composition of all minerals is listed in the electronic supplementary material (ESM 1).

**Acanthite** is one of the most common Ag minerals in the Johan de Deo vein. It is also abundant in the Goldschram-Filip vein intersection and southern part of the Priečna vein but absent in its northern part. It forms anhedral grains up to 100  $\mu\text{m}$  in association with minerals of the tetrahedrite group, polybasite, pyrargyrite, Au-Ag alloys, famatinite, and base-metal minerals (Fig. 3a, b, d). It often overgrows the older polybasite and is replaced by Cu-S minerals, uytenbogaardtite or galena of the late Ag stage. The chemical composition is characterised by lower Ag content (in comparison with ideal composition) between 1.68 and 2.04 *apfu* and S content between 0.99 and 1.26 *apfu* (probably analytical problem). Acanthite from Rudno nad Hronom contains accessory Cu up to 0.07 *apfu* and Se up to 0.02 *apfu*.

**Arsenopyrite** was identified only as a minor phase in the Johan de Deo and Anna veins. It forms euhedral

crystals associated with pyrite of the base-metal stage. Its average ( $n=7$ ) composition is  $\text{Fe}_{1.02}\text{As}_{0.93}\text{S}_{1.04}$ .

**Bornite** is abundant only in the northern part of the Priečna vein. It is mostly replacing chalcopyrite, sphalerite and galena (Fig. 3e, f). Bornite is replaced by minerals of the younger Ag-Cu stage, especially stromeyerite, mckinstryite, covellite, and chalcocite (Fig. 3f). Chemically, bornite can contain a small amount of Ag up to 0.03 *apfu*. The average empirical formula ( $n=7$ ) of bornite is  $(\text{Cu}_{4.97}\text{Ag}_{0.02})_{4.99}\text{Fe}_{1.06}\text{S}_{3.95}$ .

**Minerals of the Cu-S series** were identified at the Johan de Deo vein and Priečna vein. Covellite, digenite and chalcocite were recognised as replacing the sulfides of the base-metal stage, early Ag and late Ag stage. Based on the molar cation/anion ratio, **digenite** was identified with the ratio 1.85–1.77 (ideally 1.80), **chalcocite** with the ratio 1.89–1.96 (ideally 2.00), and **covellite** with the ratio 1.03–0.98 (ideally 1.00). Chemically, covellite does not differ from the ideal composition and contains up to 0.01 *apfu* of Ag and its crystallochemical formula is  $(\text{Cu}_{0.99}\text{Ag}_{0.01})_{1.00}\text{S}_{1.00}$ . A higher amount of Ag up to 0.10 *apfu* and Fe up to 0.08 *apfu* is present in digenite ( $n=2$ ), and its formula is  $(\text{Cu}_{8.83}\text{Ag}_{0.10}\text{Fe}_{0.08})_{9.01}\text{S}_{4.99}$ . Chalcocite differs from the ideal composition by a higher content of Ag up to 0.02 *apfu* and up to 0.05 *apfu* of Fe. The average ( $n=2$ ) empirical formula of chalcocite is  $(\text{Cu}_{1.94}\text{Ag}_{0.01}\text{Fe}_{0.04})_{1.96}\text{S}_{1.01}$ .

**Au-Ag alloys** are commonly found in minor quantities at the Priečna vein, Goldschram-Filip vein intersection and the Johan de Deo vein. They are the primary Au carriers in the Rudno nad Hronom-Brehy deposit. The Au-Ag alloys are enclosed in chalcopyrite (the northern part of the Priečna vein) and pyrite (southern part of the Priečna vein) with a grain size of up to 100  $\mu\text{m}$ . The BSE images show heterogeneity with variable Au/Ag ratio (Fig. 4a, b). The zones that appears lighter in the BSE images are richer in gold with Au/(Au+Ag) ratios ranging from 0.33 to 0.44. Silver dominates with an Au/(Au+Ag) ratio from 0.09 to 0.12 (Fig. 5) in the darker zones. Beside Au and Ag, the alloys contain minor Fe of up to 0.02 *apfu*, Cu up to 0.02 *apfu*, and Te up to 0.01 *apfu*. At the intersection of the Johan de Deo and Goldschram-Filip veins, the Au-Ag alloys form inclusions that are often found in pyrite and are affiliated to the base-metal stage. The Au-Ag alloys from this vein form grains up to 150  $\mu\text{m}$ , which are replaced along the rims by uytenbogaardtite (Fig. 4c, d). The Au/(Au+Ag) ratio of the Au-Ag alloys from the Johan de Deo and Goldschram-Filip vein intersection varies between 0.38 and 0.61.

**Famatinite** is rare and was identified only in one sample from the Johan de Deo vein. It forms anhedral grains up to 20  $\mu\text{m}$ , closely related to tetrahedrite-(Cd), argentotetrahedrite-(Cd), chalcopyrite, pyrite, sphalerite and galena. Famatinite is intensively replaced by the

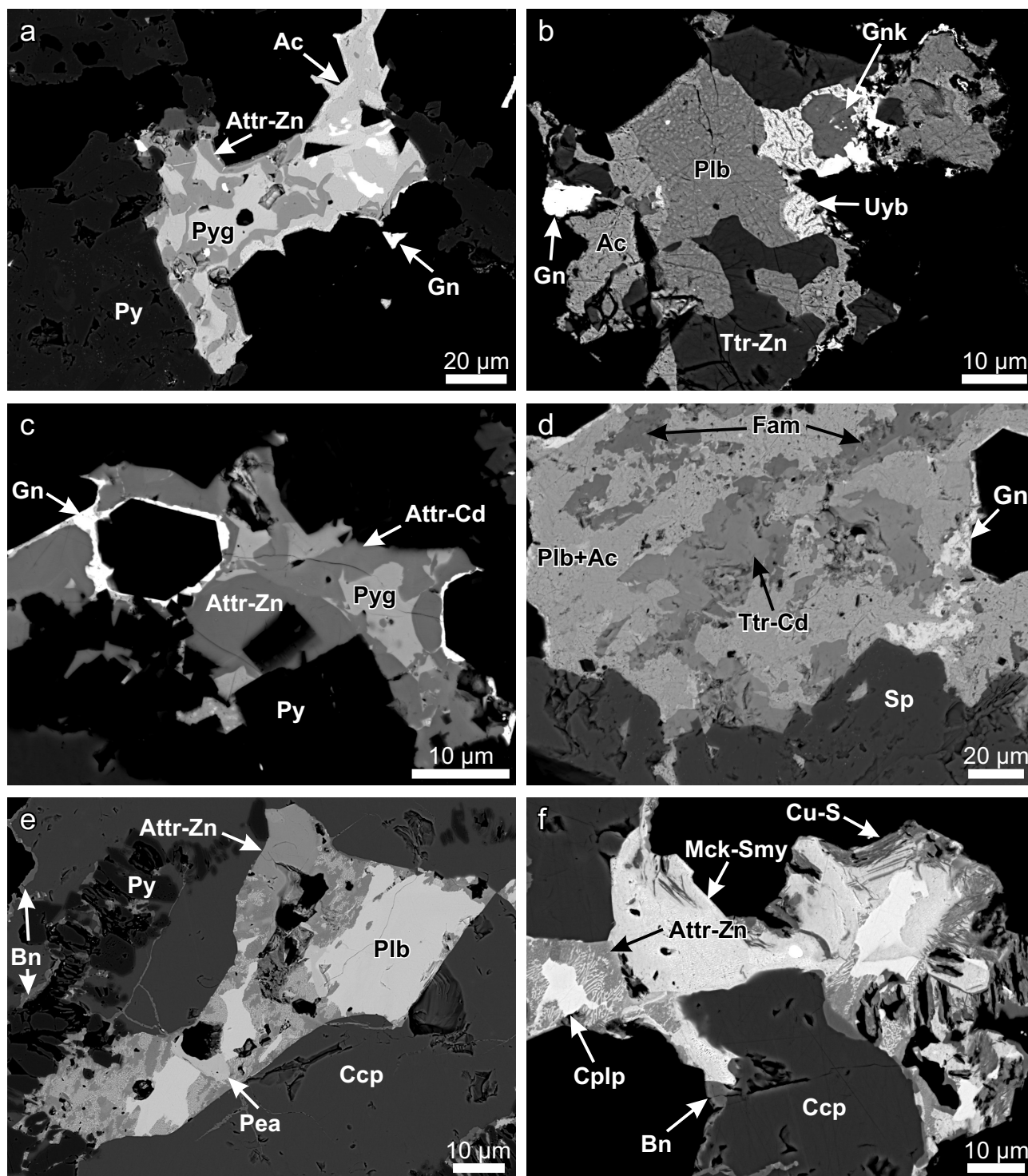


**Fig. 3** Back-scattered electron (BSE) images of ore minerals from Rudno nad Hronom-Brehy deposit. **a** – Pyrite enriched in As (Py) associated with argentotetrahedrite-(Zn) (Attr-Zn), pyrrargyrite (Pyg), acanthite (Ac) and galena (Gn) from the Johan de Deo vein. **b** – Tetrahedrite-(Zn) (Attr-Zn) with polybasite (Plb), acanthite (Ac), galena (Gn), greenockite (Gnk) and galena (Gn) from the southern part of the Priečna vein. **c** Argentotetrahedrite-(Zn) (Attr-Zn) and argentotetrahedrite-(Cd) (Attr-Cd) associated with pyrrargyrite (Pyg), galena (Gn) and pyrite (Py) from the southern part of the Priečna vein. **d** – Famatinite (Fam) and tetrahedrite-(Cd) (Ttr-Cd) replaced by the polybasite (Plb), acanthite (Ac) and galena (Gn) in association with sphalerite (Sp) from the southern part of the Priečna vein. **e** – Argentotetrahedrite-(Zn) (Attr-Zn), polybasite (Plb), pearceite (Pea) enclosed in chalcopyrite (Ccp) and pyrite (Py), replaced by bornite (Bn) from the northern part of the Priečna vein. **f** – Intergrowth of Cu-S minerals (Cu-S) with mckinstyrite (Mck) and stromeyerite (Smy) replacing cupropolybasite (Cplp), argentotetrahedrite-(Zn) (Attr-Zn) with chalcopyrite (Ccp) replaced by bornite (Bn) from the northern part of the Priečna vein.

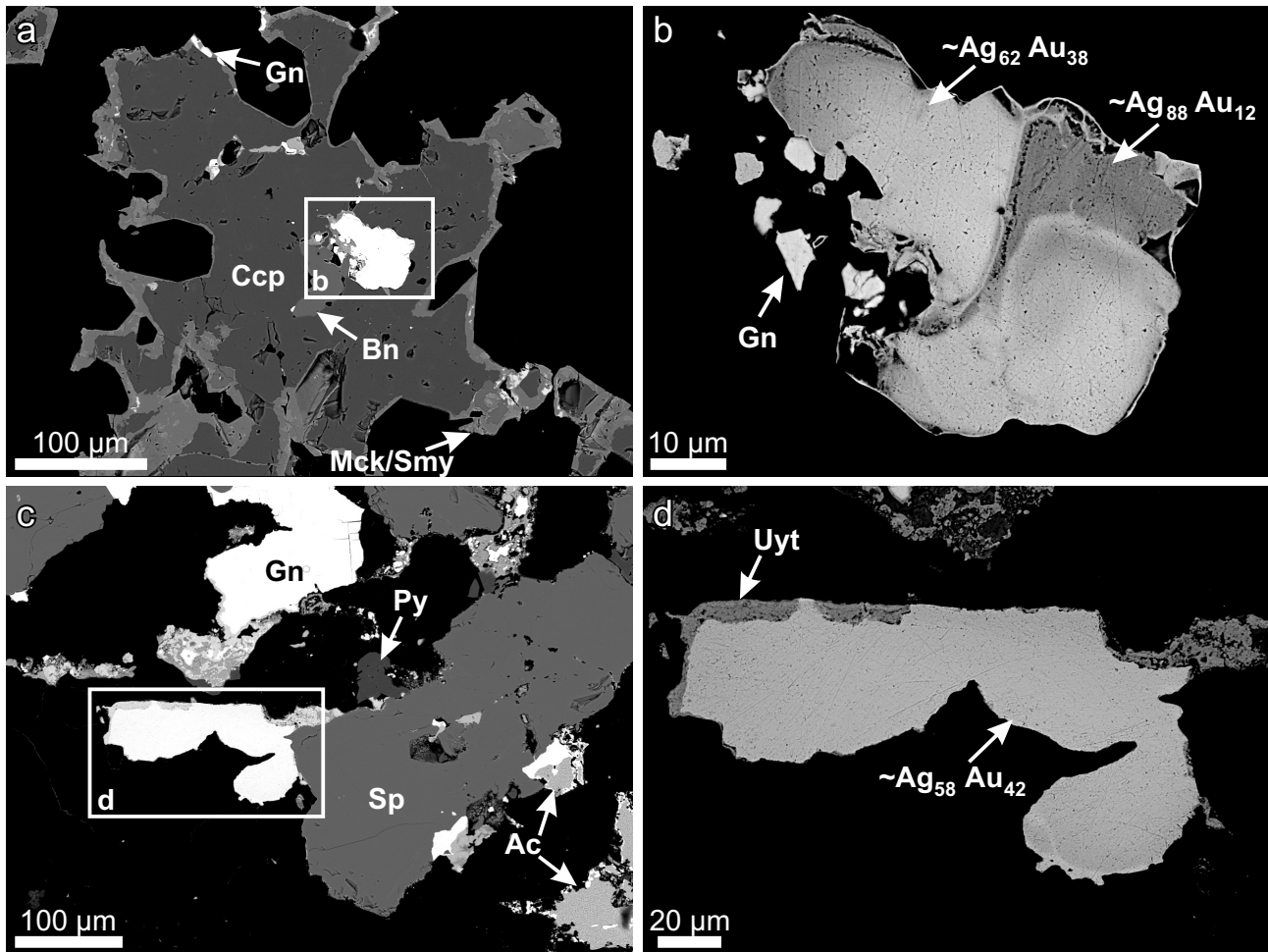


**Fig. 4** Back-scattered electron (BSE) images of ore minerals from Rudno nad Hronom–Brehy deposit. **a** – Au–Ag alloy (in the rectangle) enclosed in chalcopyrite (Ccp) replaced by bornite (Bn), galena (Gn), mckinstryite (Mck) and stromeyerite (Smy) from the northern part of the Priečna vein. **b** – Diffuse zonation of in a grain of Au–Ag alloy from the previous BSE image. **c** – Au–Ag alloy (in rectangle) associated with sphalerite (Sp), galena (Gn), pyrite (Py) and acanthite (Ac) from the southern part of the Priečna vein. **d** – Au–Ag alloy replaced by the uyttenbogaardtite (Uyt) from the previous BSE image.

minerals of the early and late Ag stage (Fig. 3d). WDS analyses show that famatinite differs only slightly from the nominal composition and contains a trace content of Fe up to 0.03 *apfu*. The mean ( $n=7$ ) empirical formula of the studied famatinite is  $(\text{Cu}_{2.95}\text{Fe}_{0.02/2.97}\text{Sb}_{1.03}\text{S}_{3.99})$ .

Base-metal minerals are represented mostly by the abundant **galena**. Galena is widespread in each vein and forms anhedral grains several tens of  $\mu\text{m}$  in size. In some cases, galena is closely associated with Au–Ag alloys and they are enclosed in pyrite. In the Anna vein, galena is the major ore mineral and forms aggregates up to 1 cm in size associated with sphalerite, chalcopyrite and pyrite. Two galena generations were identified by microscopic observation. Galena of the base-metal stage is often surrounded by younger Ag sulfides and sulfosalts, e.g., acanthite, polybasite or minerals of the tetrahedrite group. Galena as a constituent of the late Ag stage is common and appears younger than Ag sulfosalts and sulfides (Fig.

3c). Both generations of galena do not deviate much from the nominal composition PbS.

**Greenockite** occurs in the Johan de Deo and southern part of the Priečna vein and forms irregular grains up to 30  $\mu\text{m}$  in diameter (Fig. 3b). It is associated with silver sulfides and sulfosalts acanthite, uyttenbogaardtite, pyrargyrite, polybasite, argentotetrahedrite-(Zn) or argentotetrahedrite-(Cd) and tetrahedrite-(Cd). Pyrargyrite and polybasite often replace greenockite along the edges; thus, we assume its primary origin and contemporaneous precipitation with argentotetrahedrite-(Cd) or tetrahedrite-(Cd). Isometric dimorph hawleyite is described as supergene mineral phase, hence we considered hypogene origin of greenockite. The WDS analyses detected slightly increased Sb, As, Ag, Cu and Zn in greenockite.

**Chalcopyrite** is a common ore mineral in the northern part of the Priečna vein. It occurs in much lesser amounts in the other veins. In all cases, chalcopyrite belongs to

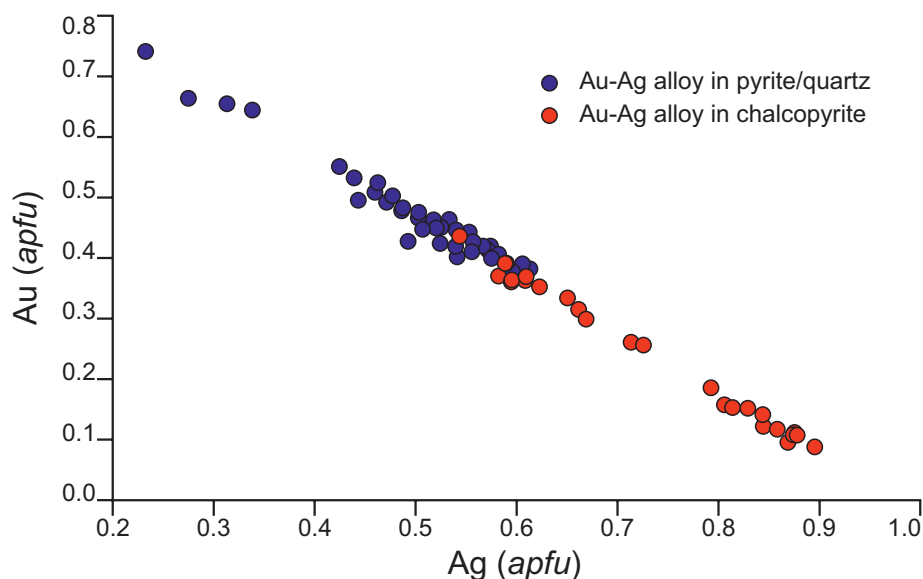


Fig. 5 Au versus Ag plot of Au–Ag alloys enclosed in chalcopyrite (northern part of the Priečna vein) and those in association with quartz and pyrite.

the base-metal stage of mineralization. In the Priečna vein, chalcopyrite occurs in the form of impregnations, with individual grain sizes up to a few millimetres in silicified breccia (Fig. 2c). Chalcopyrite fills the space between anhedral and crushed pyrite aggregates (Fig. 3e). It is intensively replaced by bornite and Cu–Ag–S minerals (mckinstryite, stromeyerite, and chalcocite) along the grain boundaries. Chalcopyrite is frequently associated with tetrahedrite-group minerals, galena and minerals of the polybasite–pearceite series (Fig. 3e, f). It commonly encloses anhedral grains of Au–Ag alloys and is overgrown by the abundant sphalerite. No chemical difference from the nominal composition of chalcopyrite was observed.

**Stromeyerite** and **mckinstryite** are common minerals of the late Ag–Cu stage of mineralization in the northern Priečna vein and form thin rims or veinlets around older

ore minerals (chalcopyrite, bornite). They often replace tetrahedrite-(Zn), tetrahedrite-(Cd) and polybasite and form myrmekites on their surface. Digenite and chalcocite seem to be younger and form thin acicular aggregates replacing stromeyerite and mckinstryite (Fig. 3f). In the Johan de Deo vein, they are found primarily in association with partially oxidised pyrite in the form of anhedral grains up to 30  $\mu\text{m}$  in association with sphalerite. The range of Ag in the minerals of mckinstryite–stromeyerite varies from 0.93 to 1.31 *apfu*, and Cu varies from 0.70 to 1.19 *apfu* (Fig. 6).

**Minerals of the cupropolybasite–cupropearceite series** are relatively rare and are only found in the northern part of the Priečna vein as part of the late Ag stage. In terms of chemical composition Cu content in cupropolybasite ranges from 4.46 to 5.90 *apfu* and in cupropearceite from 4.40 to 6.46 *apfu* (Fig. 7b). Their spatial association with abundant older chalcopyrite could mean that the fluids remobilized much Cu from the older mineralization. The chemical composition of the studied samples from the Priečna vein covers almost the complete solid solution from cupropolybasite to cupropearceite, with the molar Sb/(Sb+As) ratio ranges from 0.77 to 0.05.

Minerals of the **polybasite–pearceite series** are common

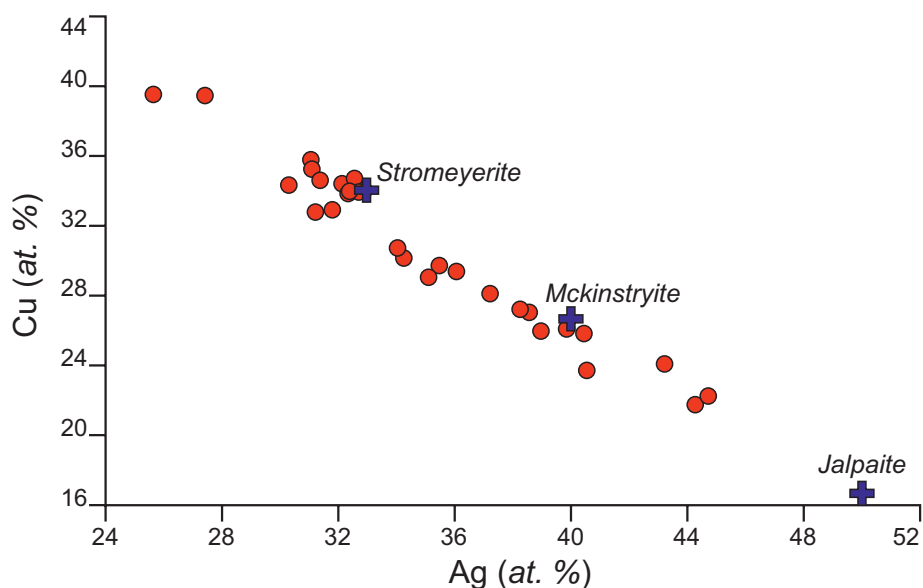
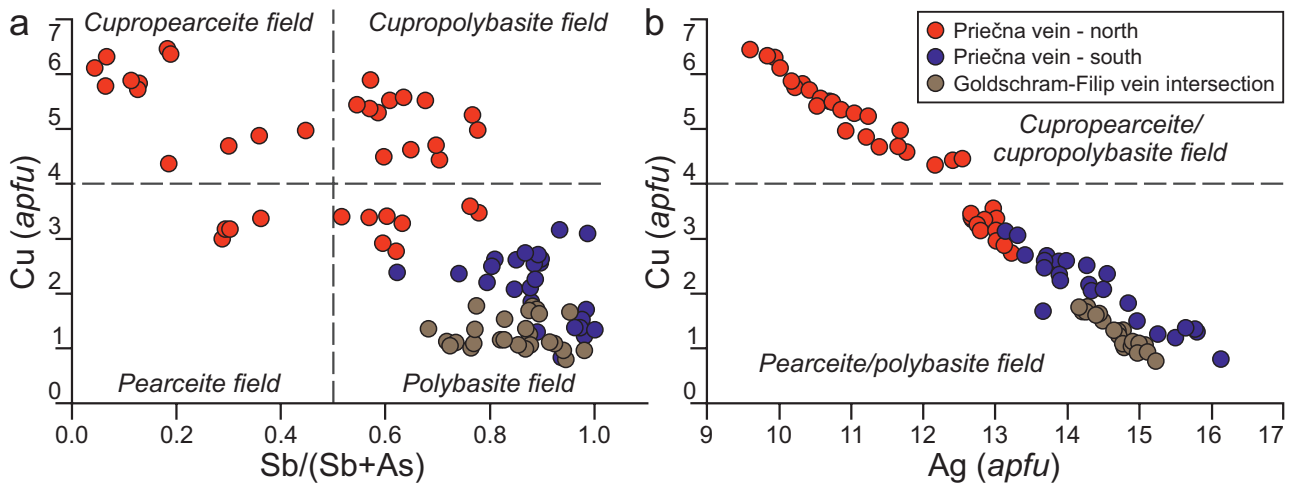


Fig. 6 Cu versus Ag plot of stromeyerite and mckinstryite from the Rudno nad Hronom and Brehy ore deposit (red dots) with the ideal composition of the end members (blue crosses).



**Fig. 7** Chemical variation of polybasite-pearceite and cupropolybasite-cupropearceite series minerals from the Rudno nad Hronom–Brehy deposit. **a** – Composition variation plot of Cu versus Sb/(Sb+As). **b** – Composition variation plot of Cu versus Ag.

Ag carriers in the veins in Rudno nad Hronom and Brehy. Composition with As > Sb (i.e., pearceite) characterizes occurrences only in the northern part of the Priečna vein (Fig. 7b). In the northern part of the Priečna vein, polybasite and pearceite fill cavities and fractures in the ubiquitous pyrite or are enclosed in chalcopyrite (Fig. 3e). Polybasite and pearceite are rarely replaced by younger mckinstryite and stromeyerite. Polybasite and pearceite are Cu and As rich in comparison with the rest of the vein systems. Cu content usually range 2.76–3.58 (Fig. 7b) *apfu* and Sb/(Sb+As) ratio ranges between 0.29 and 0.77.

In the southern Priečna vein, polybasite occurs as black euhedral tabular crystals with metallic lustre in quartz cavities, and individual crystals reach up to 0.5 cm. It is often associated with the late Ag stage galena and regularly replaces older tetrahedrite-group minerals. In the southern part of the Priečna vein the Sb/(Sb+As) ratio vary and is restricted to 0.99 to 0.62. Polybasite from the southern part of the Priečna vein is generally depleted in copper (in comparison with the northern part) which ranges 1.52–3.15 *apfu* (Fig. 7b). A minor content of Te was observed on the anion position of both members as  $\text{STe}_{-1}$  substitution, up to 0.16 *apfu*. The Fe content is very variable and rarely reaches up to 0.57 *apfu*.

In Goldschram–Filip vein intersection, polybasite occurs as up to 200  $\mu\text{m}$  anhedral grains intensively replaced by the acanthite. Polybasite from the Goldschram–Filip vein intersection is always Sb rich, with Sb/(Sb+As) ratio varies from 0.72 to 0.98. Copper content is the lowest observed among the veins in the Rudno nad Hronom and Brehy ore district and is limited to 0.79–1.78 *apfu* (Fig. 7b). Polybasite contains minor concentration of Te up to 0.02 *apfu*.

**Pyrrargyrite** occurs frequently in the Johan de Deo, Priečna vein (southern part) and in the Goldschram–Filip vein intersection. Together with acanthite, polybasite and

tetrahedrite-group minerals, it is the main Ag carrier in the late Ag stage. It forms anhedral grains up to 0.5 mm intergrown by argentotetrahedrite-(Zn) and argentotetrahedrite-(Cd) (Fig. 3a, c). Pyrrargyrite is often replaced by acanthite, polybasite and late galena. The molar Sb/(Sb+As) ratio varies in a narrow range from 0.88 to 0.97. Pyrrargyrite from Rudno nad Hronom and Brehy deposit contains a minor content of Cu up to 0.15 *apfu* and Fe up to 0.07 *apfu*.

**Pyrite** is a widespread mineral in the studied mineralization. It is often dispersed in the altered host rocks as a feature of the hydrothermal alteration. In all vein systems, pyrite preceded the main ore-forming events. In the Anna vein, euhedral to subhedral pyrite commonly appears in the breccia matrix as a dominant mineral of the pyrite stage. It is found in younger base metal stage as well. In the northern Priečna vein, pyrite is found in anhedral crushed grains up to 100  $\mu\text{m}$  overgrown by chalcopyrite and Ag sulfosalts and sulfides (Fig. 3e). In the Johan de Deo and southern section of the Priečna vein, pyrite occurs as anhedral to subhedral grains, up to 200  $\mu\text{m}$  and with variable As content. Arsenic-poor pyrite is often replaced along the edges by As-rich pyrite with <0.12 *apfu* As. In the Johan de Deo vein, pyrite is closely associated with galena and sphalerite or enclosing these minerals. It is often associated with Au–Ag alloys in the form of inclusions in the pyrite.

In the base-metal stage, **sphalerite** is a ubiquitous mineral and occurs as anhedral grains up to a few millimetres together with galena and chalcopyrite. In the Priečna vein, sphalerite is frequently coated along the edges by bornite and younger sulfide minerals of the Cu–Ag–S series. WDS analyses show a significant amount of Fe in the sphalerite from the Anna vein, reaching up to 0.10 *apfu*. In the southern part of the Priečna vein and Johan de Deo vein, Fe content in sphalerite does not

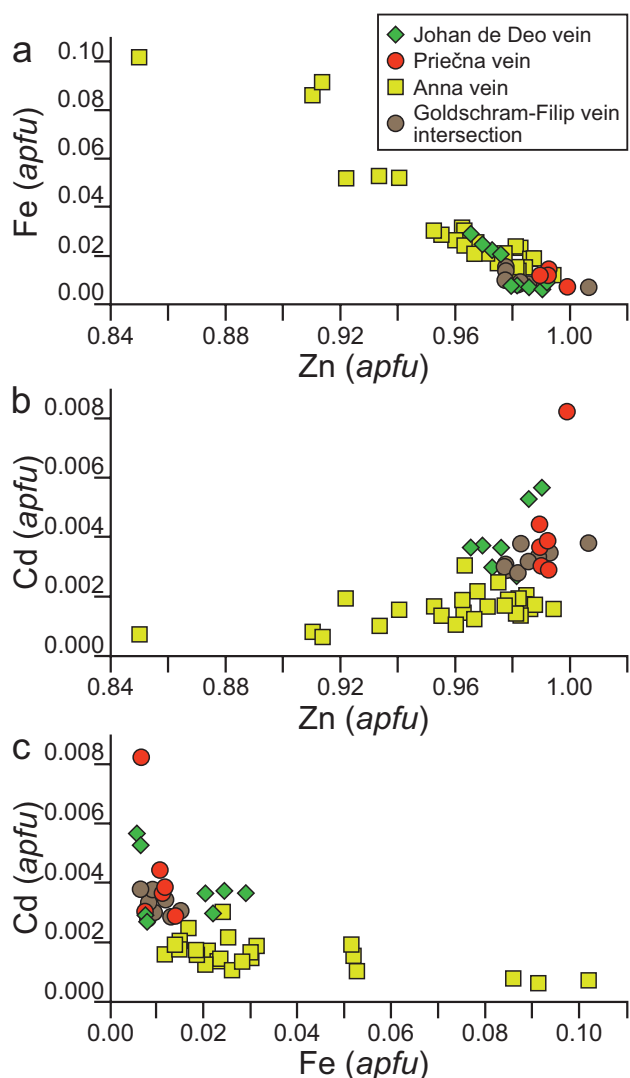


**Fig. 8** Geochemical variability of elements in sphalerite from various veins in the Rudno nad Hronom–Brehy deposit. **a** – Variation of Fe versus Zn. **b** – Variation of Cd versus Zn. **c** Variation of Cd versus Fe.

exceed 0.03 *apfu*, and in the northern Priečna vein, 0.01 *apfu* (Fig. 8). Sphalerite from the Goldschram–Filip vein intersection have similar chemical properties as Johan de Deo vein sphalerite. Beside the Fe, minor content of Cd and Mn was identified in all three vein systems, but the total amount does not exceed 0.02 *apfu*.

**Minerals of the tetrahedrite group** are common in Anna, Johan de Deo and the Priečna vein in the Rudno nad Hronom–Brehy ore deposit. They form anhedral grains and aggregates up to 200  $\mu\text{m}$  in size and in some cases with visible zonation in BSE images.

In the Anna vein, anhedral grains of tetrahedrite-(Zn) and rare tetrahedrite-(Fe) were found in close association with pyrite and older minerals of the base-metal stage as part of early Ag stage of mineralization. Chemical composition of minerals of these tetrahedrite-group minerals is rather variable (Fig. 9; nomenclature based on the Bi-

agioni et al. 2020). They contain a minor amount of Ag, and its content does not exceed 2.20 *apfu*. Tetrahedrite from the Anna vein is relatively As poor ( $<0.63$  *apfu*) and Sb/(Sb+As) ratio ranges from 0.84 to 0.94. Tetrahedrite-(Zn) shows Zn values in range of 1.09–1.42 *apfu* second dominant constituent is Fe in range of 0.56–1.01 *apfu*. The range of Fe in the tetrahedrite-(Fe) varies from 1.07 to 1.17 *apfu* and Zn content varies from 0.75 to 1.1 *apfu*. Traces of Mn were identified but do not exceed 0.02 *apfu*.

In the Johan de Deo vein, tetrahedrite-(Zn), argentotetrahedrite-(Zn) and argentotetrahedrite-(Cd) was identified (Fig. 9). In the chemical composition of tetrahedrite-(Zn), the main constituent is Cu with 7.07–9.22 *apfu* Cu, accompanied by Ag in the range 0.71–2.99 *apfu*. Zn content prevails (in range of 1.08–1.48 *apfu*) over Fe (in range of 0.61–0.95 *apfu*). Argentotetrahedrite-(Zn) contains 3.04–3.29 *apfu* of Ag with major Cu in the range from 6.72 to 7.09 *apfu*. In all cases, Zn-dominant endmembers (1.03–1.41 *apfu*) are in high portion replaced by Fe (0.94–1.00 *apfu*). Argentotetrahedrite-(Cd) contain 3.00–3.24 *apfu* of Ag and 6.86–7.03 *apfu* of Cu. Prevalent Cd content (1.68–1.86 *apfu*) is in the minority substituted by Fe (0.06–0.34 *apfu*) and Zn (0.04–0.16 *apfu*). In general, tetrahedrite-group minerals from the Johan de Deo vein are As-poor and only minor variation of Sb/(Sb+As) ratio was observed (in range 0.93–1.00).

In the Priečna vein, wide spectra of tetrahedrite-group minerals was identified, namely tetrahedrite-(Fe), tetrahedrite-(Cd), tetrahedrite-(Zn), argentotetrahedrite-(Zn) and argentotetrahedrite-(Cd). Chemical composition of the tetrahedrite-group minerals differs within the southern and northern part of the Priečna vein (Fig. 9). The Ag rich (Ag-rich members) and tetrahedrite-(Fe) are absent in the northern part. Argentotetrahedrite-(Cd) usually reaches up to 3.67 *apfu* Ag with major Cu content up to 6.98 *apfu*. High concentration of Cd (1.79–1.28 *apfu*) is accompanied by less Zn (0.02–0.46 *apfu*) and Fe (0.12–0.49 *apfu*). Silver and Cu content in argentotetrahedrite-(Zn) reaches similar values as in the argentotetrahedrite-(Cd) with values up to 3.61 *apfu* Ag and 7.07 *apfu* Cu. High Zn (1.61–1.09 *apfu*) content is substituted by non-negligible values of Fe (0.51–1.03 *apfu*). Tetrahedrite-(Fe) is relatively rare in the southern part of the Priečna vein. It is enriched in Ag up to 2.62 *apfu* and significant Cu content up to 7.73 *apfu*. Beside dominant Fe content (2.43–2.62 *apfu*), tetrahedrite-(Fe) shows high Zn values (0.74–0.91 *apfu*). In tetrahedrite-(Zn), significant differences in Ag/Cu ratio were observed between the northern and southern parts of the Priečna vein. In the northern part, tetrahedrite-(Zn) is usually Ag poor with 0.06–0.44 *apfu* Ag, whereas in the southern part, Ag content is higher, typically 2.25–2.92 *apfu*. A similar trend was recognised in the chemical composition of tetrahedrite-(Cd), where Ag content reach

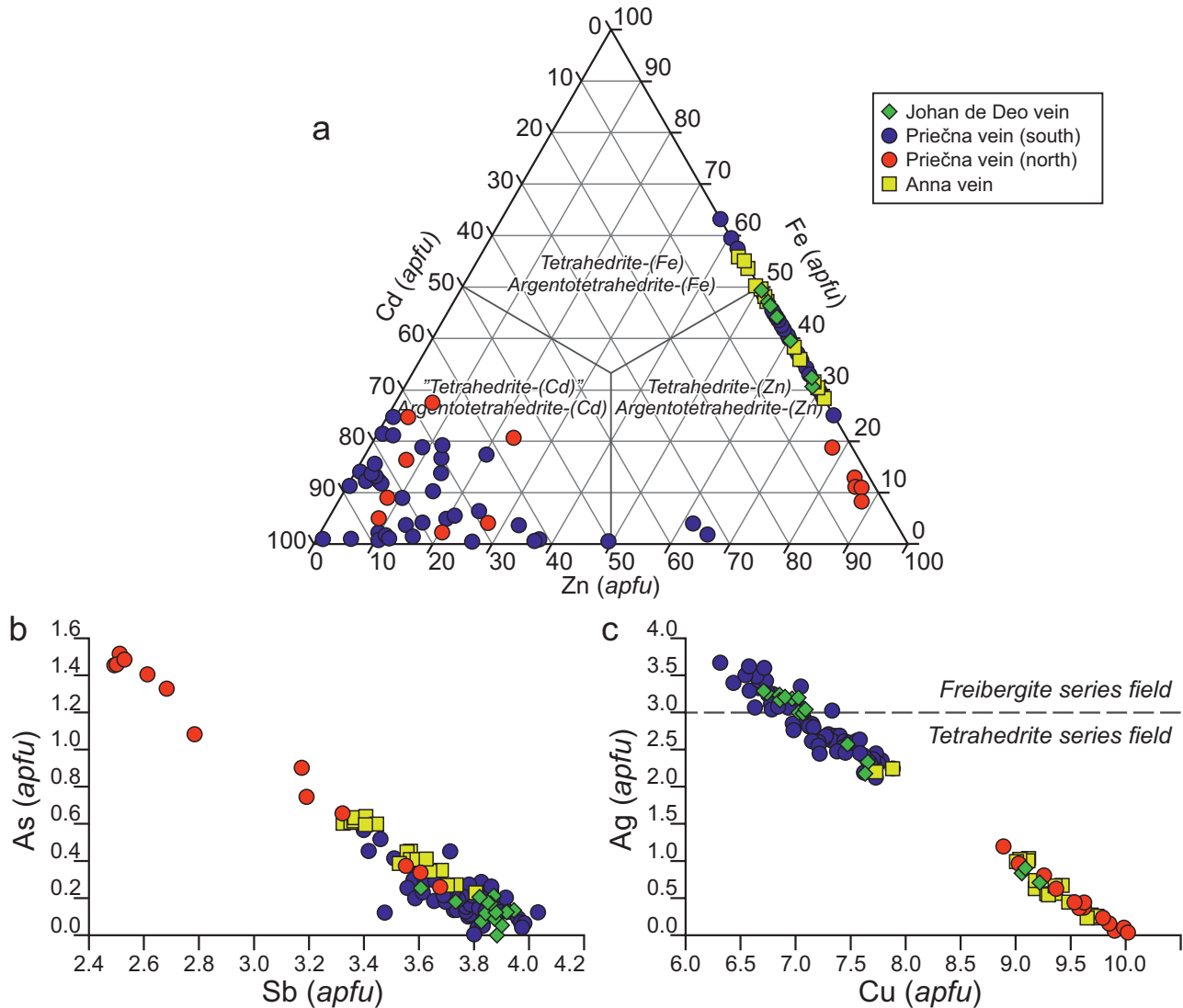


**Fig. 9** Chemical variation of tetrahedrite-group minerals from Rudno nad Hronom–Brehy deposit. **a** – Composition variation of Cd, Fe and Zn in ternary diagram. **b** – Variation of As versus Sb in tetrahedrite-group minerals. **c** – Ag versus Cu plots of geochemical variation of tetrahedrite-group minerals from the Rudno nad Hronom and Brehy veins.

0.23–1.20 *apfu* in the northern part of the vein and 2.13–2.89 *apfu* Ag in south. Another chemical difference is related to the Sb/As ratios. In the tetrahedrite-(Zn) from the northern part, the Sb/(Sb+As) ratio varies between 0.81–0.93, but between 0.93–1.00 in the southern part. Greater variation of the Sb/(Sb+As) ratios was noted in tetrahedrite-(Cd). In the northern part of the Priečna vein, this ratio varies between 0.62–0.78, whereas in the southern part between 0.86–0.97. Tetrahedrite-(Zn) from the northern part of the Priečna vein shows slightly increased Zn content (1.61–1.80 *apfu*) in the comparison with the southern part (1.01–1.43 *apfu*). On the other hand, tetrahedrite-(Cd) from the northern part of the Priečna vein contains less Cd (1.10–1.63 *apfu*) content compared to tetrahedrite-(Cd) from the southern part of the vein (0.98–1.94 *apfu*).

According to chemical variations of the tetrahedrite-group minerals and their spatial/temporal relationship, minerals of the tetrahedrite series seem to be older than the freibergite series minerals. Thus, we assume that the amount of Ag increased with time in the early Ag stage and then passes into the silver-rich late Ag stage with polybasite–pearceite group minerals, pyrrargyrite and acanthite. These Ag-rich minerals in all cases overprint the early Ag stage assemblage (Fig. 3a, c, e) and late Ag–Cu assemblage of minerals (Fig. 3f).

**Uytenbogaardtite** is found in the Johan de Deo vein and southern part of the Priečna vein, where it is a relatively frequent mineral in the late Ag–Cu stage. It is commonly associated with polybasite and acanthite or accompanied by Ag–Au alloys and rarely with greenockite (Fig. 3b). It occurs as relatively large, anhedral

Mineral	Stage				
	I. Pyrite	II. Base metal	III. Early Ag Late Ag		IV. Late Ag-Cu
Quartz/chalcedony	████████████████████				
K-feldspar	████████████████████				
Arsenopyrite	██				
Pyrite	████████████████████				
Sphalerite		████████			
Galena		████████		██	
Chalkopyrite		████████			
Electrum		██			
Famatinite			██		
Tetrahedrite-(Fe)			██		
Tetrahedrite-(Zn)			████		
Tetrahedrite-(Cd)			████		
Argentotetrahedrite-(Zn)			████		
Argentotetrahedrite-(Cd)			████		
Greenockite			██		
Pyrrargyrite				██	
Polybasite				██	
Pearceite				██	
Cupropolybasite				██	
Cupropearcite				██	
Acanthite				██	
Bornite					██
Stromeyerite					██
Mckinstryite					██
Chalcocite					██
Digenite					██
Covellite					██
Uytenbogaardtite					██

Fig. 10 Precipitation succession of the epithermal mineralization in the Rudno nad Hronom and Brehy deposit.

and porous grains up to 50 μm in size. Uytenbogaardtite from Rudno nad Hronom–Brehy contains a significant amount of Cu (up to 0.16 *apfu*) and minor amounts of Te (up to 0.03 *apfu*).

### 4.3. Evolution of ore mineralization

The epithermal mineralization in Rudno nad Hronom–Brehy deposit was formed during four stages (Fig. 10). Johan de Deo, Goldschram and Filip veins, and southern part of the Priečna vein show similar style of mineralization, different from that found in the northern part of Priečna vein and Anna vein. The main differences are: i) dominance of base-metal sulfides in the Anna vein and ii) the abundance of chalcopyrite in the northern Priečna vein.

The first, pyrite stage in all vein structures is represented by widespread pyrite with increased As content and rare arsenopyrite. The next stage is the base-metal stage with copious galena, sphalerite, and less abundant chalcopyrite. An exception, as already mentioned, is the northern part of the Priečna vein, where chalcopyrite dominates and galena is subordinate. Base-metal minerals and Au–Ag alloys together are often enclosed in pyrite in the form of inclusions or are closely spatially associated with pyrite. For this reason, we assume that the origin of base-metal sulfides and Au–Ag alloys were contemporaneous. Rare famatinite was the last mineral to precipitate in the base-metal stage.

Precipitation of Ag minerals was divided into the early Ag, late Ag, and late Ag–Cu stages. The early Ag stage commenced with argentotetrahedrite-(Zn) and tetrahedrite-(Zn), tetrahedrite-(Fe), followed by greenockite together with argentotetrahedrite-(Cd) and tetrahedrite-(Cd). Variable Ag content in the tetrahedrite group minerals indicates considerable fluctuation of silver activity in the early Ag stage ore-forming fluids. The constituents of the late Ag stage are pyrrargyrite, acanthite, and polybasite–pearceite; they all postdate the tetrahedrite-group minerals and point to higher Ag activity in the fluids. The late Ag stage resulted in the formation of galena, which occasionally form veinlets with fine-grained quartz (Fig. 2b). Late Ag–Cu stage contains an assemblage with bornite (only in Priečna vein), stromeyerite–mckinstryite, acanthite, Cu–S series minerals (digenite, chalcocite, and covellite) and uytenbogaardtite.

Weathering of the primary ores in supergene zone, reported previously by Vlasáč et al. (2021b), resulted in formation of devilline, brochantite, malachite, phosphohedyphane, mottramite, and other sulfates.

### 4.4. Bulk chemistry of the ore

Chemical analyses of samples from dumps and the vein structures accessed through the historical adits correlate well with the mineralogical observations. The entire Ag content in the analysed samples reflects the common pres-

ence of silver sulfides and sulfosalts or the minor Au–Ag alloys. Gold content is dominantly bound to the Au–Ag alloys and to a lesser extent to uytenbogaardite.

The high-grade ore samples were picked from the southern part of the Priečna vein with a maximum of 1950 ppm of Ag and 42.7 ppm of Au (sample from Fig. 2b) and from the northern part with a maximum of 1409 ppm of Ag and 9.45 ppm of Au (sample from Fig. 2c). Analyses from two unnamed samples between the Priečna vein and the Johan de Deo vein returned up to 1160 ppm of Ag and 16.1 ppm of Au. In the southern part of the Johan de Deo vein (Kršľa adit dump), high-grade ore contains up to 379 ppm of Ag and 17.4 ppm of Au (sample from Fig. 2e). Lower-grade ore was located in the intersection of Filip–Goldschram veins with a maximum of 326 ppm Ag and 4.38 ppm of Au. Waste dump material from the Filip vein (Filip adit, Beatrix adit) returned low precious metals, up to 354 ppm of Ag and 6.4 ppm of Au. Relatively low and irregularly distributed precious-metal content was observed in the surrounding mine works at Anna vein. Up to 624 ppm of Ag and 35.9 ppm of Au were identified in the rock samples from the waste dumps.

Elevated Cd content up to 42.2 ppm is caused by the presence of greenockite, tetrahedrite-(Cd) and argentotetrahedrite-(Cd). Increased As values (up to 404 ppm) probably reflect abundant arsenian pyrite, perhaps also arsenopyrite, in the samples. Minor portion of As can be derived from the Ag sulfosalts (pearceite–polybasite, pyrargyrite–proustite, and tetrahedrite). Antimony content is exclusively bound to Ag sulfosalts, and its content does not exceed 365 ppm.

In the Priečna vein, Cu content varies from the northern to the southern part of the mineralized structure. In the northern part, the ores are dominated by chalcopyrite and contain up to 5.33 wt. % of Cu. In the southern part, chalcopyrite is scarce and the ores contain only up to 608 ppm Cu. Here, the important Cu carriers are tetrahedrite, famatinite and Cu–S mineral phases (covellite, digenite and chalcocite). The southern part of the Priečna vein is richer in Pb and Zn in comparison to its northern part. Higher base-metal concentrations in the samples were detected in the samples from the Anna vein, with lower precious-metal content. Precious metals are enriched in samples with lower Pb and Zn content, which is in good agreement with the microscopic observation. The complete data set of analysed elements is listed in electronic supplementary material (ESM 2).

#### 4.5. Sulfur isotopes ( $\delta^{34}\text{S}$ )

All  $\delta^{34}\text{S}$  values measured in this study were acquired only from the base-metal stage (Fig. 11). In the later mineralization, scarcity of the sulfides and their heterogeneity precluded the measurements. The  $\delta^{34}\text{S}$  isotopic values of

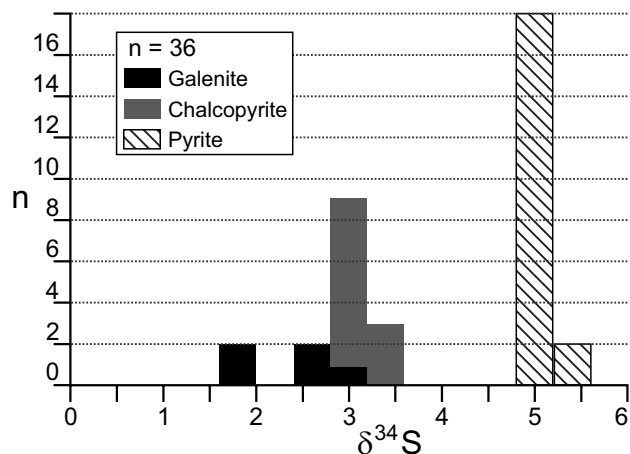


Fig. 11  $\delta^{34}\text{S}$  composition of galena, chalcopyrite and pyrite from the base-metal stage of mineralization from Rudno nad Hronom and Brehy deposit.

galena from the Anna vein vary between +1.9 ‰ to +2.5 ‰ CDT. Pyrite from the quartz veins (Anna vein) shows little variation and the  $\delta^{34}\text{S}$  values range from +4.9 ‰ to +5.2 ‰ CDT. Chalcopyrite from the Cu-rich zones of the Priečna vein yielded  $\delta^{34}\text{S}$  values between +2.8 ‰ and +3.6 ‰ CDT. The complete data set of analysed sulfur isotopes are listed in electronic supplementary material (ESM 3).

#### 4.6. Fluid inclusions

Samples for the microthermometry study were collected from the dumps of the Zubau adit targeting the Anna vein. Precious-metal mineralization in the Johan de Deo, Priečna, Filip and Goldschram veins is associated either with cryptocrystalline  $\text{SiO}_2$  forms or as impregnations in silicified hydrothermal breccia. No suitable material for the fluid inclusion study was found in these samples.

Fluid inclusions were found in quartz. They are small (<5  $\mu\text{m}$ ), two-phase, with liquid and gas. (Fig. 12). The liquid phase makes up 80–90 % of the volume of inclusions. Due to the small size, it was not possible to determine eutectic temperatures.  $T_m$  of ice ranges from –0.9 to –0.6 °C and calculated salinities vary between 1.1 and 1.6 wt. % NaCl. Homogenization temperatures (to liquid) range from 176 °C to 250 °C (Fig. 12). The calculated fluid density ranges from 0.8 to 0.9 g/cm<sup>3</sup>. No evidence of fluid boiling was recorded. We observed neither spatially associated vapour- and liquid-rich inclusions nor boiling nearly to dryness, indicated by highly saline inclusions.

#### 4.7. Hydrothermal alteration

In this work, alteration pattern was determined on the basis of mineral assemblage observation, bulk chemistry data of the samples from the drill holes (RUDD1,

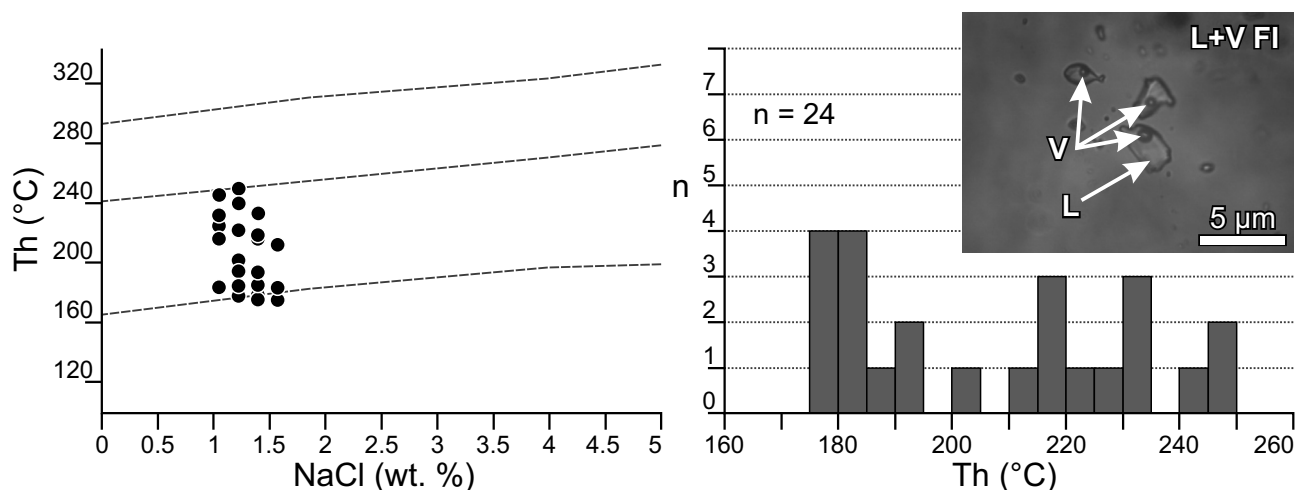


Fig. 12 Microphotograph of primary fluid inclusions composed of the vapour (V) and liquid phase (L). Plots represent the homogenisation temperature *versus* salinity of fluid inclusions and their density (dashed lines) and histogram of homogenisation temperatures.

RUDD2, and RUDD3), powder X-ray diffraction of bulk-rock samples and clay separates, and EPM analyses of alteration products.

According to the mineral assemblages two principal types of alteration have been distinguished. First, assigned to propylitization, is older, areal and pervasive. Second, potassic type of alteration is younger, developed mainly around the ore bodies (Fig. 13). In general, hydrothermal alteration in the studied area is intensive. Host rocks are exclusively andesites with groundmass and primary magmatic phenocrysts almost completely replaced by the new phases.

Propylitic rocks are typically light-grey to greenish in colour (Fig. 13a), with occasionally preserved primary plagioclase or phlogopite phenocrysts or matrix constituents. Alteration mineral assemblage comprises of quartz, chlorite, albite, smectite, carbonates (calcite, siderite), hematite and pyrite. Epidote is also present as a minor phase in the deeper parts of the deposit. Cross-cutting veinlets with white potassic alteration haloes clearly overprint propylitization (Fig. 13b). Irregular light-grey bands with no evident relationship to fissures may indicate partly pervasive character of this type of alteration (Fig. 13a). Rocks having strongest potassic alteration usually show light grey or whitish colour (Fig. 13c). Primary igneous silicates, as well as products of propylitization (particularly chlorite) are completely replaced by quartz, K-feldspar, illite/smectite and illite, carbonates (siderite), kaolinite, smectite, pyrite and marcasite. Quantitative whole-rock mineralogy (drill cores samples) of typical propylitic, potassic and mixed types of alteration is given in the electronic supplementary material (ESM 4).

**K-feldspar** is a widespread alteration mineral. It was identified in all analyzed samples in quantities ranging from 2 to 70 wt. %. Obviously, it dominates in rocks with potassic alteration. However, it is possible that negligible

amount of matrix K-feldspar having high Na content could have igneous origin. K-feldspar is intimately intergrown with quartz and pervasively replaces the matrix of the host rocks (Fig. 14a–f). Often, K-feldspar replaces phenocrysts of plagioclase (Fig. 14b), Mg–Fe silicates and oxides in association with illite, interstratified illite/smectite, smectite, kaolinite and carbonates. It commonly infills cavities of propylitized samples and occurs within haloes around the veinlets (Fig. 14c).

**Chlorite** is ubiquitous phyllosilicate in the propylitized rocks, representing up to 13 wt. % of the total mass of alteration minerals. It forms mostly at the expense of mafic phenocrysts with no remnants identifying nature of original mineral (Fig. 14d). To a lesser extent, chlorite is alteration products of plagioclase. Chlorite also replaces matrix of andesites and, in some cases, forms the part of mineralization of thin veins together with carbonates. Its Mg/(Mg + Mn + Fe) ratio varies between 0.48 and 0.57, indicating the presence of both of chamosite and clinocllore. No chlorite was identified in rocks which underwent strong K-alteration.

Another common product of alteration is **illitic material**. It consists mostly of interstratified illite/smectite (I/S), sometimes with small admixture of discrete illite. Like K-feldspar, illitic material concentrates in samples with strong K-alteration, where it can reach up to 33 wt. % of rock composition. I/S reveals exclusively R3 type of interstratification and percentage of smectite constituent (expandability) is well below 15%. Drill-core samples show inhomogeneous polytype composition when 1Md polytype absolutely prevails over 1M and 2M<sub>1</sub>. Only two samples picked directly from the vein slopes (Goldschram-Filip veins intersection) contain pure 1Md polytype. I/S alters both plagioclase and chloritized mafic phenocrysts. It is often intergrown with quartz and K-feldspar, especially in the matrix of andesitic rock (Fig. 14e, f). Relatively

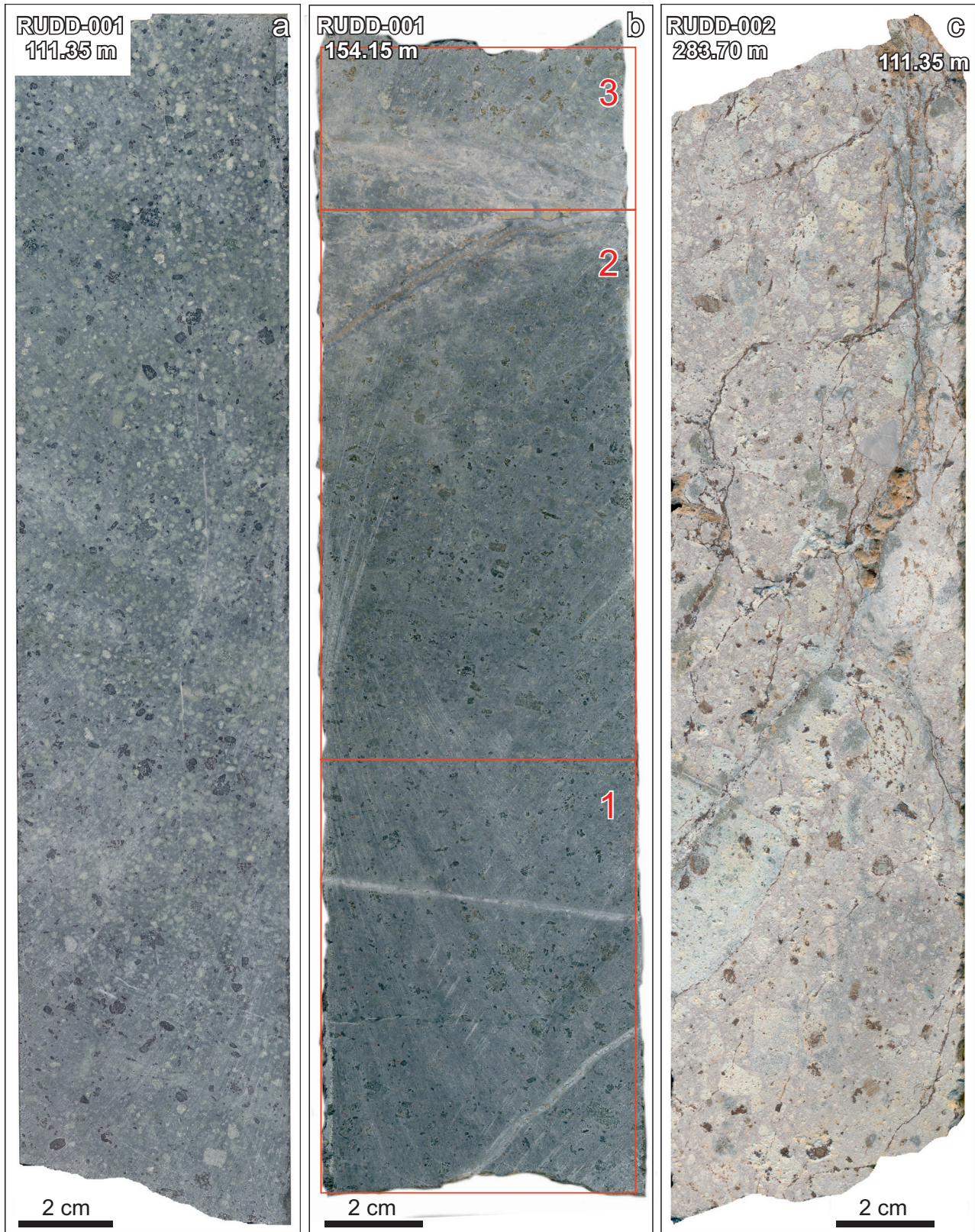


**Fig. 13** Examples of altered andesites from diamond drill cores. Left: propylitized host rocks (depth of 111.35 m); middle: rocks affected by propylitization and partially replacement by potassic alteration around the veinlets (154.15 m); right: complete replacement by potassic alteration (283.7 m). Drill core samples originated from the RUDD-001 and RUDD-002 boreholes. Red numbers and rectangles represent the parts from which powder X-ray diffraction analyses were prepared and subsequently quantified (supplementary material S4).

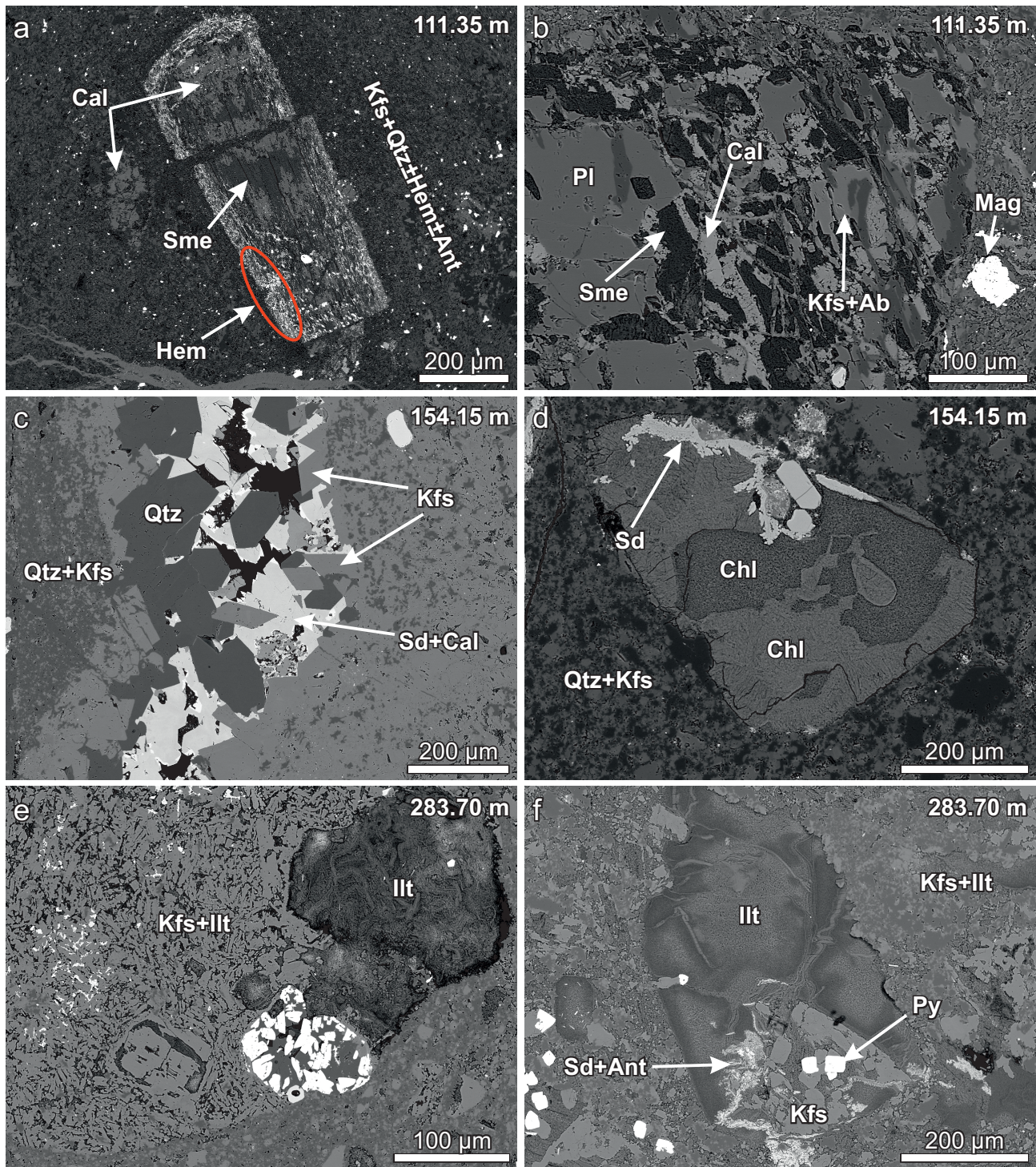


**Fig. 14** Back-scattered electron (BSE) images of sample RUDD-001 111.35 m, RUDD-001 154.15 m, RUDD-002 283.70 m (see Fig. 13). **a** – A relic of a mafic phenocryst replaced by smectite (Sme), calcite (Cal) and hematite (Hem) in K-feldspar (Kfs), quartz (Qtz) matrix with accessory hematite and anatase (Ant) **b** – A plagioclase (Pl) crystal partially replaced by smectite (Sme), calcite (Cal), K-feldspar (Kfs) and minor albite (Ab). The magnetite (Mag) crystal is most likely magmatic. **c** – A cavity in quartz (Qtz) and K-feldspar (Kfs) matrix filled with euhedral quartz and K-feldspar, siderite (Sd), calcite (Cal). **d** – A phenocryst of an igneous mineral completely replaced by chlorite (Chl) and minor siderite (Sd) in quartz (Qtz) and K-feldspar (Kfs) matrix. **e** – Phenocrysts and matrix of andesite completely replaced by a mixture of K-feldspar (Kfs) and illite (Illt) or illite/smectite, with minor quartz. **f** – A phenocryst of an igneous mineral replaced by smectite (Sme) and illite (Illt), K-feldspar (Kfs), siderite (Sd), pyrite (Py) in quartz (Qtz) and K-feldspar matrix.

**Tab. 1** K–Ar dating results from the mineral fractions of K-feldspar and interstratified illite/smectite from the drill core RUDD-001 (RUDD 1) and in clay fraction from Johan de Deo adit (RNH-1). Final ages in bold, these represent either single measurement or average of couple of measurements.

Sample	Mineral fraction	K <sub>2</sub> O (%)	Mass (mg)	K (%)	<sup>40</sup> Ar (%)	Age (Ma)
RUDD 1_143.9 m	K-feldspar	9.05	23.69	7.51	71.7	<b>12.31 ± 0.47</b>
RUDD 1_46.9 (1)	Illite/smectite (2–0.2 μm)	6.35	11.09	5.27	40.2	12.93 ± 1.10
RUDD 1_46.9 (2)	Illite/smectite (2–0.2 μm)	6.35	24.14	5.27	46.3	13.29 ± 0.92
					<b>Average:</b>	<b>13.11 ± 0.71</b>
RUDD 1_46.9 (1)	Illite/smectite (<0.2 μm)	6.47	14.79	5.37	14.7	11.54 ± 2.41
RUDD 1_46.9 (2)	Illite/smectite (<0.2 μm)	6.47	21.97	5.37	45.1	13.20 ± 0.99
RUDD 1_46.9 (3)	Illite/smectite (<0.2 μm)	6.47	19.5	5.37	37.0	12.98 ± 1.01
					<b>Average:</b>	<b>12.57 ± 0.93</b>
RUDD 1_38.7	Illite/smectite (2–0.2 μm)	6.10	13.17	5.07	51.1	<b>12.29 ± 0.86</b>
RUDD 1_38.7	Illite/smectite (<0.2 μm)	7.18	21.03	5.96	50.8	<b>12.28 ± 0.71</b>
RNH-1 (1)	Illite/smectite (2–0.2 μm)	8.03	17.42	6.67	47.5	12.29 ± 0.60
RNH-1 (2)	Illite/smectite (2–0.2 μm)	8.03	25.50	6.67	23.8	12.43 ± 1.56
					<b>Average:</b>	<b>12.36 ± 0.84</b>
RNH-1 (1)	Illite/smectite (<0.2 μm)	8.04	19.63	6.67	22.8	12.12 ± 1.64
RNH-1 (2)	Illite/smectite (<0.2 μm)	8.04	22.57	6.67	41.0	12.35 ± 0.74
					<b>Average:</b>	<b>12.24 ± 0.90</b>
					<b>Average:</b>	<b>12.45 ± 0.30</b>

common are assemblages with carbonates (calcite, siderite) and hematite, which replace Fe–Mg silicates. Variably, I/S may be intergrown with less common kaolinite. Dioctahedral smectite is omnipresent but less abundant clay mineral (<19 wt. %). In propylitic rocks it replaces phenocrysts along with chlorite, carbonates, albite and K-feldspar (Fig. 14a, b). In K-altered rocks it was found also as a part of veinlets, with K-feldspar, I/S, siderite and pyrite.

Carbonates are relatively abundant in all samples. **Siderite** is the most common for potassic alteration (up to 6 wt. %), while **calcite** is abundant in the propylitic rocks (up to 15 wt. %). They frequently replace phenocrysts of igneous minerals (Fig. 14a, b, d, and f) and occasionally they build up to 60 % of the phenocryst mass. Siderite and calcite also form fillings in the cavities and veinlets in association with quartz or K-feldspar (Fig. 14c).

**Kaolinite** is a minor clay constituent and occurs in cavities in quartz and K-feldspar almost in all studied samples. At the deepest level of the deposit, accessory **epidote** occurs with chlorites. **Pyrite** and **marcasite** in the Rudno nad Hronom and Brehy ore deposit are widespread. While pyrite is found in the form of disseminated euhedral grains, marcasite fills veinlets chiefly in the strongly altered samples. In that case, marcasite can reach up to 14 wt. % of the sample volume. **Anatase** and **hematite** are common accessory alteration products. They form small inclusions in the host-rock matrix or in the alteration mixture after the igneous mafic phenocrysts (Fig. 14a).

#### 4.8. K–Ar age of hydrothermal alteration

The age of the hydrothermal alteration that is spatially related to the studied ore bodies was determined by the K/Ar radiometric method. Isotopic data were acquired

mainly from the illitic material of two different grain-size fractions (<0.2 μm and 2–0.2 μm). In one case, K-feldspar was also dated. Samples used for K/Ar dating comes from potassic alteration zones, exclusively. Quantitative mineral compositions of dated separates are shown in supplementary material (supplementary material S5).

Practically the same K–Ar ages of thicker (2–0.2 μm) and finer (<0.2 μm) fractions, within uncertainties, in the case of all samples indicates no detrital or thicker older component, which would lead to older ages of thicker fractions. Potassium bearing minerals in both fractions of one sample: K-feldspar, illite 2M<sub>1</sub> and illite 1Md – illite–smectite are therefore having the same ages. The age interval of hydrothermal alteration from the drill core RUDD1 which targeted Anna vein is 12.6 ± 0.9–13.1 ± 0.9 Ma with a mean value of 12.8 ± 0.7 Ma. Analyses from the Filip–Goldschram veins intersection show values in the interval from 12.2 ± 0.9 Ma to 12.4 ± 0.8 Ma with a mean of 12.3 ± 0.6 Ma. The grand average age of all analyses is 12.5 ± 0.3 Ma (Tab. 1). Observed data reveal relatively high errors. To evaluate the analytical precision, it should be noted that the content of radiogenic <sup>40</sup>Ar is very low in some cases, leading to high uncertainties. The problem may lie in the fact that dated clay-size fractions of illitic material uniformly contained high amounts smectite and kaolinite and therefore, amounts of K and radiogenic <sup>40</sup>Ar was lower.

## 5. Discussion

Epithermal mineralizations have been divided into high-, intermediate-, and low-sulfidation type (Hedenquist et al. 2000). The nature of alteration patterns, low-saline fluid

inclusions, scarcity of carbonate gangue and common cryptocrystalline quartz point to the low-sulfidation type of an epithermal deposit (Hedenquist et al. 2000; Sillitoe and Hedenquist 2003; Simmons et al. 2005). Low-sulfidation properties of Rudno nad Hronom–Brehy mineralization, including association with rhyolitic volcanism, were described during the exploration of the area in the last century (Štohl et al. 1993). However, the abundance of tetrahedrite-group minerals and lack (or scarcity) of pyrrhotite, arsenopyrite, and selenide assemblage point to the intermediate sulfidation state of mineralization (Wang et al. 2019). The presence of famatinite can even suggest higher sulfidation conditions (Arribas 1995). Tetrahedrite group minerals and famatinite are common only in the early stage of deposit development. At this point, we can assume change in sulfidation state of mineralization from intermediate- to low-sulfidation condition.

Hydrothermal alteration assemblages are commonly regularly zoned around vein or breccia-filled fluid conduits. However, they may be regularly zoned in near-surface environments or where permeable rocks have been replaced. Alteration mineralogy that includes K-feldspar, carbonates and interstratified illite/smectite or illite is characteristic of low- and intermediate-sulfidation deposits formed from geothermal systems and indicates near-neutral pH to alkaline fluids (Simpson and Mauk 2011; John et al. 2003, 2018; Kouhestani et al. 2020). K-feldspar and illite or I/S rich association of hydrothermal alteration forms in a hydrothermal system where surficial waters mix with deeper and heated waters (Heald et al. 1987).

Precious-metal mineralization in Rudno nad Hronom–Brehy deposit is characterised by a high Ag: Au ratio (average 85: 1; Fig. 15). Similar low-sulfidation epithermal

veins related to Miocene volcanism are located throughout the Central Slovak volcanic field, e.g., in Nová Baňa, Hodruša, Kremnica or Pukanec (Bahna and Chovan 2001; Majzlan 2009; Berkh et al. 2014; Majzlan et al. 2018; Števkó et al. 2018). Selenides and tellurides are common observed in the various Štiavnica stratovolcano related epithermal veins, but in the veins in Rudno nad Hronom–Brehy deposit missing (e.g. Kremnica, Števkó et al. 2018 or Hodruša, Kubač et al. 2018; Chovan et al. 2019). The base-metal mineralization is a common initial ore deposition stage feature in the central parts of the Miocene rocks of the Štiavnica stratovolcano (Koděra et al. 2005) or in the Kremnica epithermal deposit (Böhmer 1966; Števkó et al. 2018).

Carbonates (calcite, siderite) are common in the alteration products in the host rocks but absent in the vein filling. Quartz and chalcedony are the prevalent gangue minerals. Similar Au–Ag ores depleted in carbonates were found in some horst-related veins in the Hodruša–Hámre ore district, e.g., Rabenstein, where the early carbonates were completely replaced by late quartz (Majzlan et al. 2016). A similar situation was described from Nová Baňa Au–Ag mineralization (4 km NW from studied locality), where only quartz pseudomorphs after carbonates were found (Majzlan et al. 2018). A different case was described from the Pukanec Au–Ag epithermal veins (3.5 km S from the studied locality), where rodochrosite and calcite are common gangue along the quartz (Bahna and Chovan 2001). Precious-metal ore mineralizations in the central part of Štiavnica stratovolcano are usually carbonate-rich. Massive carbonate veins are located in the Schöpfer vein with common bladed calcite and in some parts the calcite veins reach thickness of 20 m (Majzlan et al. 2016 and citations mentioned therein).

In the Finsterort and Anton veins, beside quartz carbonates like calcite, siderite and dolomite are the main gangue minerals (Vlasáč et al. 2021a). In the Bieber vein (Štiavnica ore district), quartz and carbonates are prevalent and K-feldspars are less common (Chovan et al. 2021).

The Rudno nad Hronom–Brehy deposit has some paragenetic similarities with the Nová Baňa deposit, located approximately 4 km northwest. Strong

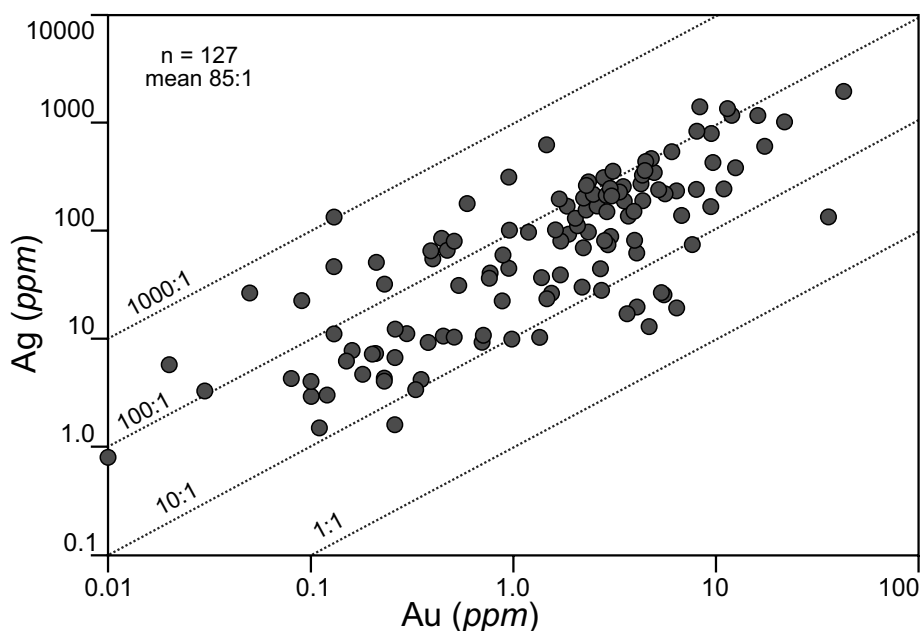


**Fig. 15** Concentration of Au and Ag and Ag:Au ratio in grab samples from Rudno nad Hronom–Brehy deposit. Both axes are converted to the logarithmic scale.

chemical zonality of mineralization was discovered in the Nová Baňa, where bottom parts were enriched in base metal with high Cu content and increased Au volume but weak enrichment in Ag. In the uppermost parts of the veins, the Ag: Au ratio can commonly exceed 100:1, sometimes even 1000:1. The average Ag: Au ratio for the entire deposit Nová Baňa is 64:1 (Majzlan et al. 2018). In the Banská Štiavnica ore district Koděra and Hvožd'ara (1960) defined vertical zonality of the veins according the thermality and dominant metal contents. Near-surface low-thermal are usually enriched in Pb–Zn (galena, sphalerite) and rhodonite, intermediate-thermal central parts of the veins contain except Pb and Zn, zones rich in Cu and high temperature bottoms are dominant Cu-rich. Chalcopyrite is dominant in the Cu zone and is considered as genetically younger than minerals of the Pb–Zn zone (Koděra and Hvožd'ara 1960).

Pyrite from the Rudno nad Hronom and Brehy ore deposit is often enriched in As. This anomaly was found at the Rabenstein occurrence (Hodruša) with occasional As zonation of pyrite (common in the Rudno nad Hronom and Brehy), which indicates variations in the composition of ore-forming fluids (Berkh et al. 2014). High As content in pyrite were found in the ore dressing product from the Rozália mine, however only pyrite from the altered rocks contains As, whereas pyrite in the hydrothermal veins does not (Chovan et al. 2016).

Blanchard et al. (2007) demonstrated that a considerable amount of As that can be present in the pyrite rims (up to 10 wt. %), that substitute for S in the structure of pyrite. Pyrite from the Rudno nad Hronom–Brehy deposit (from the pyrite stage of mineralization) contains up to 0.12 apfu (7.26 wt. %) of As. Pyrite from the high-sulfidation deposits can incorporate arsenic as an  $As^{3+}$  cation (Chouinard et al. 2005). The As and S concentrations in the studied pyrite are inversely correlated (Fig. 16), thus complying with  $As^{-}S^{-}$  substitution typical for reducing

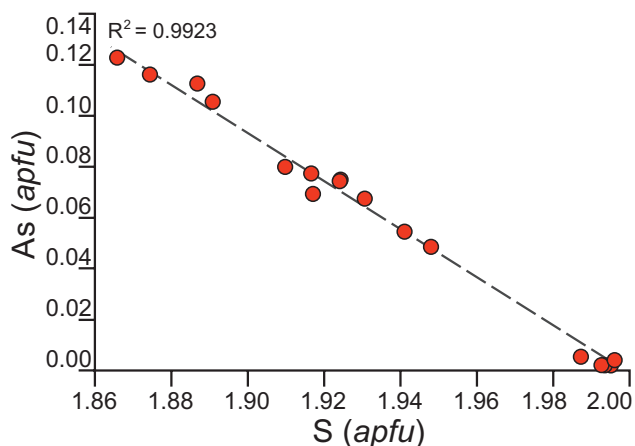


Fig. 16 Negative correlation of As and S in pyrite from Rudno nad Hronom and Brehy deposit.

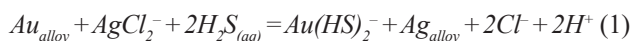
environments (Blanchard et al. 2007; Reich et al. 2013; Morishita et al. 2018).

An interesting feature of the studied mineralization is the spatial zonation of the As concentration among one vein and even among the distinct vein systems mainly in the minerals of the early and late Ag stage. The northern part of the Priečna vein is As-rich with the typical mineral assemblage enriched in As, namely pearceite, cupropearceite and tetrahedrite-(Cd), tetrahedrite-(Zn) with increased As content. However, there is less As in its southern part and pyrrargyrite is common. The depleted As concentration (in tetrahedrite-(Fe), tetrahedrite-(Zn), polybasite) is observed in the Johan de Deo, Anna vein and the Goldschram–Filip vein intersection.

A typical feature for the mineralization in the Rudno nad Hronom–Brehy is the presence of cadmium. In this work, we identified three minerals containing Cd as a major element: argentotetrahedrite-(Cd), tetrahedrite-(Cd) and greenockite. Rudno nad Hronom is the type locality for argentotetrahedrite-(Cd) (Mikuš et al. 2023). The rarity of Cd-bearing minerals in epithermal systems is not only related to the low Cd crustal abundance (0.102  $\mu\text{g/g}$ ; Wedepohl 1995) but also to its preference to partition into the structures of chalcopyrite and sphalerite. It is difficult to determine the cadmium source in the mineralization; however, one option is that it originates from the bituminous shales or coal matter of the Upper Carboniferous of Hronic Unit, which has been drilled and confirmed by the deep borehole GK-15 in the Brehy area (Bray et al. 1977). The mean cadmium content of bituminous shales reported worldwide is 0.80 g/t (Waketa and Schmidt 1978). Cadmium volume in the coals ranges widely and is reported to be 0.01 to 180 g/t in the US (Valkovic 1983), up to 2.0 g/t in bituminous coals in Australia (Swaine 1977) and up to 22 g/t worldwide (Bowen 1979). The following are examples of mean cadmium content in the volcanic rocks by Waketa and Schmidt (1978) and citations mentioned therein: 0.017 g/t in andesites, 0.27 g/t in rhyolite and 0.07 g/t in granodiorite.

The isotopic composition of sulfur ( $\delta^{34}\text{S}$ ) in the sulfide of ore mineralization is influenced by the isotopic composition of the source material and the fluid-mineral fractionation. The latter is governed by pressure, temperature, the strength of metal–sulfur bonds in sulfides, oxygen fugacity and Eh–pH of hydrothermal fluids (Ohmoto 1972; Ohmoto and Rye 1979; O'Neil 1986; Hoefs 2015). Sulfides of the base-metal stage in the Rudno nad Hronom–Brehy ore deposit have a narrow range of  $\delta^{34}\text{S}$ , caused by the stable physicochemical conditions of their formation and a homogenous source of sulfur (Ohmoto and Rye 1979). In general, sulfur in low-sulfidation ores with precious-metal minerals has a magmatic source ( $\delta^{34}\text{S}$  of  $-5$  to  $+5$  ‰ range) or a mixture of magmatic and host-rock sulfur (Herbert and Smith 1978; Castor et al. 2003).

Most of the gold grains (primarily at the Priečna vein) show diffuse zonality of the Au/Ag ratios within single grains. Gammons and Williams-Jones (1995) considered the chemical equilibrium that describes precipitation (eq. 1), identifying the parameters that control the Au/Ag chemical variability of precipitated Au-Ag alloy:



Increasing  $Ag_{\text{alloy}}$  is accompanied by decreasing temperature (through equilibrium constant), decreasing  $Au/Ag_{\text{aq}}$ , increasing pH, decreasing  $aCl^-_{(\text{aq})}$  and subsequently increasing  $aH_2S$ . Most of these parameters usually change during the evolution of a hydrothermal system. For example, decreasing  $aH_2S$  in solution and falling temperature have a contrasting effect on the value of  $Au/Ag_{\text{alloy}}$ . On the other hand, relatively stable local mineralization conditions (in terms of P–T–X) should generate Au–Ag alloys showing evident homogeneity (e.g., Johan de Deo vein, Filip vein, and Goldschram vein; Chapman et al. 2021).

### 5.1. Evaluation of ore-forming and hydrothermal alteration temperature

Field and textural evidences suggest that ore forming process was accompanied with strong potassic alteration of host, already propylitized andesitic rocks. Thus, mineral products of potassic alteration could be useful for characterization of ore forming fluids. Clay minerals are good indicators of the temperature conditions of host rock alteration. Smectite is stable at  $<130^\circ\text{C}$ , interstratified illite-smectite (I/S) at  $130$  to  $230^\circ\text{C}$  and illite at  $>230^\circ\text{C}$  (Steiner 1968; Browne and Ellis 1970; Reyes 1990; Harvey and Browne 1991; Simmons and Browne 2000). In our samples, smectite and I/S are abundant, but illite is scarce. Therefore, we assume formation temperature for the illitic clays  $<230^\circ\text{C}$ . Temperatures obtained from empirical I/S geothermometry ( $177$ – $224^\circ\text{C}$ ; Šucha et al. 1993) are in good agreement with temperature estimates from active geothermal systems ( $150$ – $220^\circ\text{C}$ ; Steiner 1977; Reyes 1990). Low- to intermediate-sulfidation systems with the mineral assemblage illite, smectite, chlorite, mixed-layered clays, pyrite, calcite and quartz develop at  $180^\circ\text{C}$  to  $220^\circ\text{C}$  (Hedenquist et al. 2000; Leavitt and Arehart 2005; Syafrizal and Watanabe 2007; John et al. 2018). However, it should be noted here that the clay geothermometry is strongly influenced by the metastable behavior of clays and is not based on equilibrium reactions (Essene and Peacor 1995). From that point of view, an error may occur in temperatures in the range of  $30$ – $60^\circ\text{C}$ . The presence of epidote in deeper parts of propylitized rocks may indicate higher temperature  $>240^\circ\text{C}$  for this type of alteration (Harvey and Browne 1991).

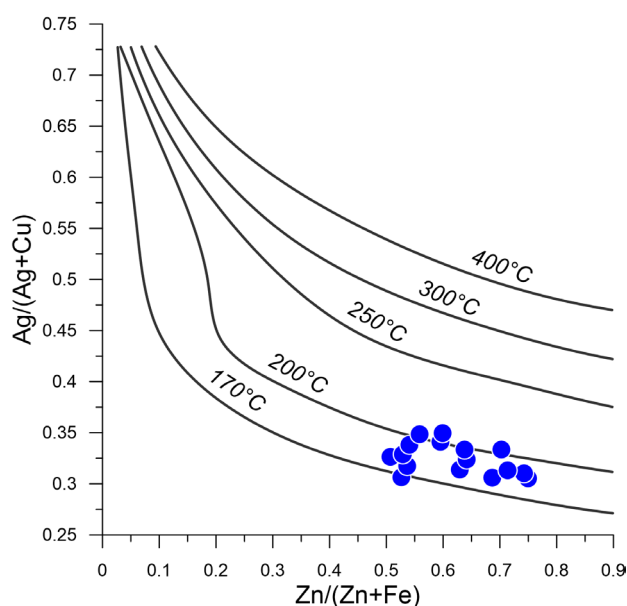


Fig. 17 Isotherms of the tetrahedrite geothermometer (after Sack 2005; Sack and Ebel 2006) with plotted molar  $Ag/(Ag + Cu)$  and  $Zn/(Zn + Fe)$  ratios in argentotetrahedrite-(Zn) from Rudno nad Hronom and Brehy.

The fluid inclusion data show total homogenization temperatures between  $176^\circ\text{C}$  to  $250^\circ\text{C}$  and bulk salinities of  $1.1$  to  $1.6$  wt. % NaCl eq. These parameters might imply that mineralization of the base-metal stage involved mixing and cooling with meteoric fluids.

The chemical composition of argentotetrahedrite (Zn and Fe end members) depends on the temperature and, thus, may be used for geothermometry (Sack 2005; Hernández and Akasaka 2010). The database for sulfides and sulfosalts in the system  $Ag_2S$ – $Cu_2S$ – $ZnS$ – $Sb_2S_3$ – $As_2S_3$  developed by Sack (2005) can be used to estimate crystallisation temperature of the argentotetrahedrite. According to the molar ratio of  $Ag/(Ag + Cu)$  and  $Zn/(Zn + Fe)$  of argentotetrahedrite-(Zn), the estimated temperature of the early Ag stage is roughly  $170$ – $205^\circ\text{C}$  (Fig. 17).

The absence of stephanite in the late Ag stage may impose an upper limit on the formation temperatures in this stage. Stephanite decomposes in the absence of sulfur to form pyrargyrite + argentite at  $197 \pm 5^\circ\text{C}$  (Keighin and Honea 1969). However, epithermal pyrargyrite-proustite exhibit complete As–Sb solid solution at temperatures of deposition, which can suggest temperature  $<160^\circ\text{C}$  (Motomura 1990; Bindi et al. 2010).

The fast reaction rates of solid solution encountered throughout the system Cu–Ag–S demonstrate that very few of the observed assemblages are likely to preserve an unaltered record of specific conditions of ore formation, even in supergene processes. Even at room temperature, reactions proceed at observable rates, and partial conversions may be obtained in a few days (Skinner 1966). The late Ag–Cu stage was formed below  $118.9^\circ\text{C}$  because the

minerals present (mckinstryite, stromeyerite and jalpaite) are stable only below this temperature (Wu 1987). Mckinstryite breaks down at  $94.4 \pm 1.5$  °C to a two-phase intergrowth of jalpaite ( $\text{Ag}_3\text{CuS}_2$ ) and a cation-disordered *hcp* phase of composition  $\text{Ag}_{1.04}\text{Cu}_{0.96}\text{S}$  (Kolitsch 2010). All reported occurrences of mckinstryite were interpreted to be the result of a low-temperature (stable up to 94 °C) formation of either hypogene or supergene character. Skinner (1966) reported invariant points for low-temperature assemblages in the Cu–Ag–S system. Stromeyerite + chalcocite can be stable at 67 °C. Digenite with covellite is stable up to 76 °C. Stromeyerite + mckinstryite are stable up to 90 °C, whereas stromeyerite breaks down at 93 °C. Jalpaite with acanthite is stable up to 106 °C.

Uytenbogaardtite occurs in association with electrum and/or acanthite and its deposition is either late hydrothermal (low-temperature) or has been formed in the supergene stage (alteration stage). Thermodynamic modelling supports the idea that this mineral can originate at low temperatures (as low as 25 °C), even if the fluids are relatively oxidising (Palyanova, Savva 2008).

### 5.2. Age of hydrothermal alteration linked to the evolution of the Štiavnica stratovolcano

Our age determination of K-feldspar and clay minerals associated with the ore mineralization in the Rudno nad Hronom–Brehy ore deposit yielded an average age of  $12.8 \pm 0.7$  Ma from the drill core samples RUDD-001 (targeting Anna vein) and an average age of  $12.3 \pm 0.6$  Ma from the Filip–Goldschram vein intersection. These ages correlate well with the radiometric dating of rhyolite volcanism (Jastrabá formation) accompanied by the long-lasting uplift of the resurgent horst. In general, according to previous studies on epithermal mineralization, precious-metal and base-metal veins in the Central Slovakia Volcanic Field are related to rhyolite volcanism (Kovalenker et al. 1991; Onáčila et al. 1995; Chernyshev et al. 1995; Lexa et al. 1999; Háber et al. 2001; Lexa and Pécskay 2010; Chernyshev et al. 2013). The temporal interval of the rhyolite volcanism was determined as  $12.3 \pm 0.4$  to  $12.0 \pm 0.4$  Ma (Lexa and Pécskay 2010); more recent research using K–Ar and Rb–Sr geochronological methods yielded an age of rhyolite volcanism in the interval of  $12.2 \pm 0.8$  to  $11.4 \pm 0.4$  Ma (Chernyshev et al. 2013). According to the volcanic evolution of the Štiavnica stratovolcano, rhyolite volcanism belongs to the fifth stage of its formation (Konečný and Lexa 2000; Chernyshev et al. 2013). Kraus et al. (1999) confirmed that the process of hydrothermal precious- and base-metal mineralization in the Banská Štiavnica and the Kremnica stratovolcanoes took place approximately within the period of  $12.5 \pm 0.1$  and  $11.0 \pm 0.1$  Ma.

## 6. Conclusions

- 1) The ores in the Rudno nad Hronom–Brehy area are bound to silicified hydrothermal breccias and the thin chalcedony veins with disseminated Au–Ag-rich mineralization. The precious metal content in the richest parts of the veins ranges up to 1950 ppm Ag and 42.7 ppm Au, and the overall average ratio of Ag: Au is 85:1. Base-metal mineralization is represented to a greater extent in the deeper parts of the deposit (Anna vein). Precious-metal mineralization was a significant resource of the deposit with variable volume of Au–Ag alloys, tetrahedrite-(Zn), argentotetrahedrite-(Zn), tetrahedrite-(Cd), argentotetrahedrite-(Cd), tetrahedrite-(Fe), pyrrargyrite, polybasite, pearceite, cupropearceite, cupropolybasite, acanthite, stromeyerite, mckinstryite and uytenbogaardtite.
- 2) In the Rudno nad Hronom–Brehy deposit, four ore-forming stages were recognised. Immediately after the initial pyrite stage, the homogenization temperature of fluid inclusions of base-metal stage ranges of 176–250 °C. The third stage is divided into two sub-stages. The ore-forming temperatures of the early Ag stage (based on argentotetrahedrite-(Zn) and argentotetrahedrite-(Fe) geothermometer) are 170–205 °C and those for the late Ag stage with galena (based on the mineral phase stability) are <160 °C. The late Ag–Cu stage (based on the mineral phase stability) formed at temperatures <93 °C.
- 3) Sulfides of the base-metal stage in the Rudno nad Hronom–Brehy ore deposit have a relatively narrow range of  $\delta^{34}\text{S}$ . This observation is interpreted by stable physicochemical conditions of their formation and a homogenous source of sulfur.  $\delta^{34}\text{S}$  isotopes suggest an igneous source or a mixture of igneous and host-rock sulfur.
- 4) The degree of hydrothermal alteration varies from propylitic to potassic. Alteration affected the andesitic host rocks and progressively removed the primary igneous minerals. In the proximity of the ore, the host rock is pervasively silicified and replaced by K-feldspar and interstratified illite–smectite; the igneous minerals are no longer preserved in the fragments of altered rocks in the hydrothermal breccias. Propylitic and potassic altered rocks are compositionally distinguished by the presence of chlorite (chamosite, clinocllore) and illite, smectite, interstratified illite/smectite ratio. Carbonatization (calcite and siderite) is widespread in each of the alteration types. Calcite is most abundant in propylitic alteration, whereas siderite in the potassic mineral association. Pyritization is abundant in all alteration type. Anatase and hematite are frequent accessories in each sample. The temperature of formation of the hydrothermal alteration

according to the illite/smectite geothermometer is up to 224 °C.

- 5) An age determination of K-feldspar and clay minerals associated with the ore mineralization in the Rudno nad Hronom–Brehy ore deposit yielded an average age of  $12.8 \pm 0.7$  Ma from the drill core samples RUDD-001 (targeting Anna vein) and an average age of  $12.2 \pm 0.6$  Ma from the Filip–Goldschram vein intersection. The grand average of all analyses is  $12.5 \pm 0.3$  Ma. Ore mineralization in the Rudno nad Hronom–Brehy deposit is temporally and spatially related to the initial stage of local horst uplift. It could be also genetically linked to the rhyolite volcanism (Jastrabá fm.) of the fifth stage of Štiavnica stratovolcano evolution.
- 6) According interpretation of obtained mineralogical and geochemical data, we can assume transition from intermediate- to low-sulfidation condition of epithermal mineralization. The style of mineralization in the Rudno nad Hronom–Brehy deposit exhibit similar features suchlike mineralization in the Nová Baňa deposit.

*Acknowledgements.* The authors thank Peter Tuček and Jakub Bukovina (Prospech Ltd, Banská Štiavnica) for their help with the field work. The study was financially supported by the Ministry of Education, Science, Research and Sport of the Slovak Republic (projects VEGA 2/0028/20, VEGA 2/0029/23 and APVV-22-0041). The reviewer Jiří Sejkora and the handling editor Jiří Zachariáš are highly acknowledged for their constructive comments and suggestions that improved the manuscript.

## References

- ARRIBAS A (1995) Characteristics of high-sulfidation epithermal deposits, and their relation to magmatic fluid. In: THOMPSON JFH (ed) *Magmas, fluids, and ore deposits*. Mineralogical Association of Canada Short Course, vol. 23, pp 419–454
- BAHNA B, CHOVAN M (2001) Low-sulfidation type of epithermal Au–Ag mineralization near Pukanec (central Slovakia Neogene volcanic field). *Geolines* 13: 11–17
- BAKKER RJ (2018): *AqSo\_NaCl*: computer program to calculate  $p$ – $T$ – $V$ – $x$  properties in the  $H_2O$ – $NaCl$  fluid system applied to fluid inclusion research and pore fluid modelling. *Comput Geosci* 115: 122–133
- BAKOŠ F, FUCHS P, HANES R, ŽITŇAN P, KONEČNÝ V (2010) Au-porphyry mineralization in the mantle of the Štiavnica stratovolcano (Western Carpathians). *Miner Slov* 42: 1–14
- BERGFEST A (1953) Rudno (pyrite). Unpublished report, State Geological Institute of Dionýz Štúr, Bratislava: 1–44 (in Slovak)
- BERKH K, MAJZLAN J, CHOVAN M, KOZÁK J, BAKOŠ F (2014): Mineralogy of the medieval Ag–Au occurrences Banská Belá, Treiboltz, Rabenstein, and Kopanice in the Banská Štiavnica ore district (Slovakia). *Neu Jb Mineral, Abh* 191: 237–256
- BIAGIONI CH, GEORGE LL, COOK NJ, MAKOVICKÝ E, MOELO Y, PASERO M, SEJKORA J, STANLEY CH J, WELCH MD, BOSI F (2020) The tetrahedrite group: Nomenclature and classification. *Amer Miner* 105: 109–122
- BINDI L, PRATESI G, SPRY PG (2010) Crystallographic and chemical constraints on the nature of the proustite–pyrrhotite solid–solution series. *Amer Miner* 95: 1725–1729
- BLANCHARD M, ALFREDSSON M, BRODHOLT J, WRIGHT K, CATLOW CRA (2007) Arsenic incorporation into  $FeS_2$  pyrite and its influence on dissolution: A DFT study. *Geochim Cosmochim Acta* 71: 624–630
- BODNAR RJ (1993) Revised equation and table for determining the freezing point depression of  $H_2O$ – $NaCl$  solutions. *Geochim Cosmochim Acta* 57: 683–684
- BOWEN HJM (1979) *Environmental chemistry of the Elements*. Academic Press, London, pp 1–320
- BÖHMER M (1966) Geology and mineral associations of gold-bearing veins in the central part of the Kremnica ore field. *Acta Geol Geogr Uni Comen Geol* 11: 5–123
- BRLAY A, MIHALIKOVÁ A, VOZÁR J, POLÁK M, ŠKVARKA J (1977) Metalogenetic research of Central Slovakia neovolcanites – structural borehole GK-15-Brehy. Unpublished report, State Geological Institute of Dionýz Štúr, Bratislava: 1–261 (in Slovak)
- BROWNE PRI, ELLIS AJ (1970) The Ohaki–Broadlands hydrothermal area, New Zealand. Mineralogy and related geochemistry. *Amer J Sci* 269: 97–131
- BRUKER AXS (2010) *DIFRAC.EVA – User Manual*, Bruker AXS, Karlsruhe, Germany: 1–134
- CASTOR SB, BODEN DR, HENRY CD, CLINE JS, HOFSTRA AH, MCINTOSH WC, TOSDAL RM, WOODEN JP (2003) The Tuscarora Au–Ag district: Eocene volcanic-hosted epithermal deposits in the Carlin gold region, Nevada. *Econ Geol* 98: 339–366
- DRIESNER T, HEINRICH CA (2007) The system  $H_2O$ – $NaCl$ . Part I: Correlation formulae for phase relations in temperature–pressure–composition space from 0 to 1000 °C, 0 to 5000 bar, and 0 to 1 xNaCl. *Geochim Cosmochim Acta* 71: 4880–4901
- DUDEK T, RODOŇ J (1996) Identification of illit/smectite by X-ray powder diffraction taking into account lognormal distribution of crystal thickness. *Geol Carpath – Clays* 5: 21–32
- EBERL DD (2003) *User guide to RockJock – A program for determining quantitative mineralogy from X-ray diffraction data*. U.S. Geological Survey Open-File Report, OF 03-78: 1–40
- ESSENE EJ, PEACOR DR (1995) Clay mineral thermometry – a critical perspective. *Clays Clay Miner* 43: 540–553

- GAMMONS CHH, WILLIAMS-JONES AE (1995) Hydrothermal geochemistry of electrum; thermodynamic constraints. *Econ Geol* 90: 420–432
- HÁBER M, JELEŇ S, KOVALENKER VA, CHERNYSHEV IV (2001) Model of epithermal ore mineralization of the Banská Štiavnica ore district. *Miner Slov* 33: 215–224 (in Slovak with English abstract)
- HARVEY CC, BROWNE PRI (1991) Mixed-layer clay geothermometry in the Wairakei geothermal field, New Zealand. *Clays Clay Miner* 39: 614–621
- HEALD P, FOLEY NK, HAYBA DO (1987) Comparative anatomy of volcanic-hosted epithermal deposits. Acid-sulfate and adularia-sericite types. *Econ Geol* 82: 1–26
- HEDENQUIST JW, ARRIBAS AR, GONZALES-URIEN E (2000) Exploration for epithermal gold deposits, Chapter 7. In: Hagemann SG, Brown PE (eds) *Gold in 2000*. Society of Economic Geologists, *Rev Econ Geol* 13: 245–27
- HERBERT H, SMITH J (1978) Sulfur isotopes and origin of some sulfide deposits, New England, Australia. *Miner Depos* 13: 51–63
- HERNÁNDEZ ANG, AKASAKA M (2010) Ag-rich tetrahedrite in the El Zancudo deposit, Colombia: occurrence, chemical compositions and genetic temperatures. *Resour Geol* 60: 218–233
- HILLIER S (1999) Use of an air brush to spray dry samples for X-ray powder diffraction. *Clay Miner* 34: 127–135
- HOEFS J (2015) *Stable isotope geochemistry*, 7<sup>th</sup> edition. Springer International Publishing, Switzerland, pp 1–286
- CHAPMAN RJ, BANKS DA, STYLES MT, WALSHAW RD, PIAZOLO S, MORGAN DJ, GRIMSHAW MR, SPENCE-JONES CP, MATTHEWS TJ, BOROVINSKAYA O (2021) Chemical and physical heterogeneity within native gold: implications for the design of gold particle studies. *Miner Depos* 56: 1563–1588
- CHERNYSHEV IV, HÁBER M, KOVALENKER VA, IVANENKO VV, JELEŇ S, KARPENKO MI (1995) The age of the magmatic events and epithermal Au–Ag base metals mineralization in the central zone of the Banská Štiavnica Stratovolcano: K/Ar data. *Geol Carpath* 46: 327–334
- CHERNYSHEV IV, KONEČNÝ V, LEXA J, KOVALENKER VA, JELEŇ S, LEBEDEV VA, GOLTSMAN YV (2013) K–Ar and Rb–Sr geochronology and evolution of the Štiavnica Stratovolcano (Central Slovakia). *Geol Carpath* 64: 327–360
- CHOUINARD A, PAQUETTE J, WILLIAMS-JONES AE (2005) Crystallographic controls on trace-element incorporation in auriferous pyrite from the Pascua epithermal high-sulfidation deposit, Chile–Argentina. *Canad Mineral* 43: 951–963
- CHOVAN M, JÁGERSKÝ I, DELANEY V, ŽITŇAN P, KUBAČ A, BAČÍK P, TROPPOVÁ D, MIKUŠ T (2016) Mineralogy of ore dressing products from Banská Hodruša Au (Ag, Pb, Cu) epithermal deposit. *Acta Geol Slov* 8: 203–216
- CHOVAN M, KUBAČ A, MIKUŠ T, ŽITŇAN P, PRCÚCH J (2019) Au–Ag tellurides and sulphosalts from epithermal Au–Ag–Pb–Zn–Cu deposit Banská Hodruša at the Rozália mine (Slovakia). *Acta Geol Slov* 11: 43–62
- CHOVAN M, MIKUŠ T, PRCÚCH J, BAČA B (2021) Assemblage of Ag–Pb–Bi±Cu sulfosalts from the Bieber vein, Banská Štiavnica deposit, Slovakia. *Acta Geol Slov* 13: 191–198
- JOHN DA, HOFSTRA AH, FLECK RJ, BRUMMER JE, SADERHOLM EC (2003) Geological setting and genesis of the Mule Canyon low-sulfidation epithermal gold–silver deposit, north-central Nevada. *Econ Geol* 98: 425–464
- JOHN DA, VIKRE PG, DE BRAY EA, BLAKELY RJ, FEY DL, ROCKWELL BW, MAUK JL, ANDERSON ED, GRAYBEA FT (2018) Descriptive models for epithermal gold–silver deposits. U.S. Geological Survey Scientific Investigations Report 2010-5070-Q: 1–247
- KEIGHIN CW, HONEA RM (1969) The system Ag–Sb–S from 600 °C to 200 °C. *Miner Depos* 4: 153–171
- KELLET D, JOYCE N (2014) Analytical details of the single- and multicollection <sup>40</sup>Ar/<sup>39</sup>Ar measurements for conventional step-heating and total-fusion age calculation using the Nu Noblesse at the Geological Survey of Canada. Geological Survey of Canada, Technical Note, 8, pp 1–27
- KODĚRA M, HVOŽDARA P (1960) About paragenetic research of Štiavnica–Hodruša and Vyhne ore district in the 1958 and 1959. Scientific-research institute geologically geographical, Comenius university, Bratislava: 1–178 (in Slovak)
- KODĚRA P, LEXA J, RANKIN AH, FALICK AE (2004) Fluid evolution in a subvolcanic granodiorite pluton related to Fe and Pb–Zn mineralization, Banská Štiavnica ore district, Slovakia. *Econ Geol* 99: 1745–1770
- KODĚRA P, LEXA J, FALICK AE (2010) Formation of the Vysoká–Zlatno Cu–Au skarn–porphyry deposit, Slovakia. *Miner Depos* 45: 817–843
- KODĚRA P, LEXA J, FALICK AE, WÄLLE M, BIROŇ A (2014) Hydrothermal fluids in epithermal and porphyry Au deposits in the Central Slovakia Volcanic Field. Geological Society, London, Special Publications 402: 177–206
- KODĚRA P, LEXA J, RANKIN AH, FALICK AE (2005) Epithermal gold veins in a caldera setting: Banská Hodruša, Slovakia. *Miner Depos* 39: 921–943
- KOLITSCH U (2010) The crystal structure and compositional range of mckinstyrite. *Mineral Mag* 74: 73–84
- KONEČNÝ V (1971) Evolutionary Stages of the Banská Štiavnica Caldera and Its Post-volcanic Structures. *Bull Volcanol* 35: 95–116
- KONEČNÝ V, LEXA J (2000) Structure and evolution of the Neogene Štiavnica stratovolcano (Central Slovakia). *Miner Slov* 32: 217–220
- KONEČNÝ V, LEXA J, HALOUZKA R, HÓK J, VOZÁR J, DUBLAN L, NAGY A, ŠIMON L, HAVRILA M, IVANIČKA J, HOJSTRIČOVÁ V, MIHALIKOVÁ A, VOZÁROVÁ A, KONEČNÝ P, KOVÁČIKOVÁ M, FILO M, MARCIN D, KLUKANOVÁ A, LIŠČÁK P, ŽÁKOVÁ E (1998a) Explanations to the Geological Map of the Štiavnické Vrchy and Pohronský Inovec

- Mountains (Štiavnica Stratovolcano) 1 : 50 000, I. and II. Part. Geological Survey of Slovak Republic, Bratislava, pp 1–473 (in Slovak with English summary)
- KONEČNÝ V, LEXA J, HALOUZKA R, DUBLAN L, ŠIMON L, STOLÁR M, NAGY A, POLÁK M, VOZÁR J, HAVRILA M, PRISTAŠ J (1998b) Geological map of Štiavnica Mts. and Pohronský Inovec Mts. (Štiavnica stratovolcano). Geological Survey of Slovak Republic, Bratislava
- KOUHESTANI H, MOKHTARI MAA, QIN K, ZHANG X (2020) Genesis of the Abbasabad epithermal base metal deposit, NW Iran: Evidence from ore geology, fluid inclusion and O–S isotopes. *Ore Geol Rev* 126: 103752
- KOVALENKER VA, JELEŇ S, LEVIN KA, NAUMOV BV, PROKOFIEV VY, RUSINOV VL (1991) Mineral assemblages and physico-chemical model of the formation of gold–silver–polymetallic mineralization on the deposit Banská Štiavnica (Central Slovakia). *Geol Carpath* 42: 291–302
- KOZÁK J, KODĚRA P, LEXA J, BAKOŠ F, MOLNÁR L, WÄLLE M (2017) Porphyry gold system of Beluj in the mantle of the Štiavnica stratovolcano (Slovakia). *Acta Geol Slov* 9: 45–61
- KRAUS I, CHERNYSHEV IV, KOVALENKER VA, LEBEDEV VA, ŠAMAJOVÁ E (1999) Use of illite for K–Ar dating of hydrothermal precious and base metal mineralization in Central Slovak Neogene volcanic rocks. *Geol Carpath* 50: 1–12
- KUBAČ A, CHOVAN M, KODĚRA P, KYLE JR, ŽITŇAN P, LEXA J, VOJTKO R (2018) Mineralogy of the epithermal precious and base metal deposit Banská Hodruša at the Rozália Mine (Slovakia). *Mineral Petrol* 112: 705–731
- LEAVITT ED, AREHART GB (2005) Alteration, geochemistry, and paragenesis of the Midas epithermal gold–silver deposit, Elko County, Nevada. In: RHODEN HN, STEININGER RC, VIKRE, PG (eds) *Geological Society of Nevada Symposium 2005: Window to the World*, Reno, Nevada, May 2005: 563–627
- LEE JY, MARTI K, SEVERINGHAUS JP, KAWAMURA K, YOO HS, LEE JB., KIM JS (2006) A redermination of the isotopic abundances of atmospheric Ar. *Geochim Cosmochim Acta* 70: 4507–4512
- LEXA J, SMOLKA J (2002) Ore district Rudno–Brehy–Pukanec. In: LEXA J (ed) *Metallogenetic evaluation of Slovak Republic area*. Unpublished report, State Institute of Dionýz Štúr, Bratislava: 1–25 (in Slovak)
- LEXA J, PÉCSKAY Z (2010) Radiometric dating of rhyolites by conventional K–Ar method: methodical aspects. In: KOHÚT M (ed) *Dating of minerals and rocks, metamorphic, magmatic and metallogenetic processes, as well as tectonic events*. ŠGÚDŠ, Bratislava: 21–22
- LEXA J, ŠTOHL J, KONEČNÝ V (1999) The Banská Štiavnica ore district: relationship between metallogenetic processes and the geological evolution of a stratovolcano. *Miner Depos* 34: 639–654
- MAJZLAN J (2009) Ore mineralization at the Rabenstein occurrence near Banská Hodruša, Slovakia. *Miner Slov* 41: 45–54
- MAJZLAN J, BERKH K, KODĚRA P, ŠTEVKO M, BAKOS F, MILOVSKÝ R (2016) A mineralogical, fluid inclusion, and isotopic study of selected epithermal Ag–Au occurrences in the Banská Štiavnica–Hodruša–Hámre ore district, Western Carpathians. *Acta Geol Slov* 8: 133–147
- MAJZLAN J, BERKH K, KIEFER S, KODĚRA P, FALLICK AE, CHOVAN M, BAKOŠ F, BIROŇ A, FERENC Š, LEXA J (2018) Mineralogy, alteration patterns, geochemistry, and fluid properties of the Ag–Au epithermal deposit Nová Baňa, Slovakia. *Mineral Petrol* 112: 1–23
- MIKUŠ T, VLASÁČ J, MAJZLAN J, SEJKORA J, STECIUK G, PLÁŠIL J, RÖSSLER C, MATTHES C (2023) Argentotetrahedrite-(Cd), Ag<sub>6</sub>(Cu<sub>4</sub>Cd<sub>2</sub>)Sb<sub>4</sub>S<sub>13</sub>, a new member of the tetrahedrite group from Rudno nad Hronom, Slovakia. *Mineral Mag* DOI 10.1180/mgm.2022.138
- MOORE DM, REYNOLDS RC (1997) *X-Ray Diffraction and the Identification and Analysis of Clay Minerals*. Second Edition. Oxford University Press, pp 1–378
- MORISHITA Y, SHIMADA N, SHIMADA K (2018) Invisible gold in arsenian pyrite from the high-grade Hishikari gold deposit, Japan: significance of variation and distribution of Au/As ratios in pyrite. *Ore Geol Rev* 95: 79–93
- MOTOMURA Y (1990) Solid solution ranges for pyrargyrite–proustite series minerals in the Inakuraishi-type manganese deposits of Japan. *Ganko: Ganseki Kobutsu Kosho Gakkai shi* 85: 502–513 (in Japanese with English abstract)
- ODIN GS (1982) How to measure glaucony ages? In: ODIN GS (ed) *Numerical Dating in Stratigraphy*. Wiley, pp 387–403
- OHMOTO H (1972) Systematics of sulfur and carbon isotopes in hydrothermal ore deposits. *Econ Geol* 67: 551–578
- OHMOTO H, RYE R (1979) Isotopes of sulfur and carbon. In: BARNES HL (ed) *Geochemistry of Hydrothermal ore Deposits – Second Edition*. John Wiley & Sons, New York, USA, pp 506–567
- ONAČILA D, LEXA J, MARSINA K, ROJKOVIČOVÁ L, KÁČER Š, HOJSTRIČOVÁ V, ŽÁKOVÁ E, ŠTOHL J, KONEČNÝ V, NEMČOK M, KODĚRA P, REPČOK I, HURAI V, HÁBER M, JELEŇ S, MAŤO Ľ (1995) Metallogenetic model and prognostic evaluation of the central zone of the Štiavnica stratovolcano. Unpublished report, Geological Survey of Slovak Republic, Bratislava: 1–231 (in Slovak)
- O'NEIL JR (1986) Theoretical and experimental aspects of isotopic fractionation. In: VALLEY W, O'NEIL JR (eds) *Stable isotopes in high temperatures geological processes*. *Rev Mineral* 16: 1–40
- PALYANOVA GA, SAVVA NE (2008) Some sulfides of gold and silver: Composition, mineral assemblage, and conditions of formation. *Theor Found Chem Eng* 42: 749–761
- REICH M, DEDITIUS A, CHRYSOULIS S, LI J-W, MA CH-Q, PARADA MA, BARRA F, MITTERMAYR F (2013) Pyrite as a record of hydrothermal fluid evolution in a porphyry

- copper system: A SIMS/EMPA trace element study. *Geochim Cosmochim Acta* 104: 42–62
- REPČOK I (1982) Dating of West Carpathian Neogene volcanism by the uranium division footprint method. Unpublished report, Geological Survey of Slovak Republic, Bratislava: 1–65 (in Slovak)
- REYES AG (1990) Petrology of Philippine geothermal systems and the application of alteration mineralogy to their assessment. *J Volcanol Geotherm Res* 43: 279–309
- REYNOLDS RC JR (1980) Interstratified clay minerals. In: BRINDLEY GW, BROWN G (eds) *Crystal Structure of Clay Minerals and Their X-Ray Identification*. Monograph No. 5, Mineralogical Society, London: 249–303
- ROEDDER E (1984) *Fluid Inclusions*. De Gruyter, Berlin, Boston, pp 1–646
- ROTTIER B, AUDÉTAT A, KODĚRA, P, LEXA J (2020) Magmatic evolution of the mineralised Štiavnica volcano (Central Slovakia): Evidence from thermobarometry, melt inclusions, and sulfide inclusions. *J Volcanol Geotherm Res* 401: 106967
- SACK RO (2005) Internally consistent database for sulfides and sulfosalts in the system  $Ag_2S$ – $Cu_2S$ – $ZnS$ – $FeS$ – $Sb_2S_3$ – $As_2S_3$ : Update. *Geochim Cosmochim Acta* 69: 1157–1164
- SACK RO, EBEL DS (2006) Thermochemistry of sulfide mineral solutions. *Rev Mineral Geochem* 61: 265–364
- SILLITOE R, HEDENQUIST J (2003) Linkages between volcanotectonic settings, ore fluid compositions, and epithermal precious metal deposits. *Society of Economic Geologists, Special Publication* 10: 315–343
- SIMMONS SF, BROWNE PRL (2000) Hydrothermal minerals and precious metals in the Broadlands–Ohaaki geothermal system: Implications for understanding low-sulfidation epithermal environments. *Econ Geol* 95: 971–999
- SIMMONS SF, WHITE NC, JOHN DA (2005) Geological characteristics of epithermal precious and base metal deposits. *Society of Economic Geologists, Economic Geology 100<sup>th</sup> Anniversary Volume*: 485–522
- SIMPSON MP, MAUK JL (2011) Hydrothermal alteration and veins at the epithermal Au–Ag deposits and prospects of the Waitakauri area, Hauraki Goldfield, New Zealand. *Econ Geol* 106: 945–973
- SKINNER BJ (1966) The system Cu–Ag–S. *Econ Geol* 61: 1–26
- SMOLKA J, SKAVINIAK M, VALKO P, KÁMEN M, DAUBNER J, PETR K, GWERK E, NOVÁK P, KOVÁČ P, RUŽIAKOVÁ B, MJARTANOVÁ H (1988) Final report of the project Rudno–Brehy–Pukanec. Unpublished report, Geological Survey of Slovak Republic, Bratislava: 1–108 (in Slovak)
- STEINER A (1968) Clay minerals in hydrothermally altered rocks at Wairakei, New Zealand. *Clays Clay Miner* 16: 193–213
- STEINER A (1977) The Wairakei geothermal area, North Island, New Zealand. *New Zealand Geological Survey Bulletin* 90: 1–136
- SWAINE DJ (1977) Trace elements in coal. In: HEMPHILL DD (ed) *Trace substances in environmental health*, University of Missouri, Columbia, XI: 107–116
- SYAFRIZAL IMAI A, WATANABE K (2007) Origin of ore-forming fluids responsible for gold mineralization of the Pongkor Au–Ag deposit, west Java, Indonesia: Evidence from mineralogical, fluid inclusion microthermometry and stable isotope study of the Ciurug-Cikoret veins. *Resour Geol* 57: 136–148
- ŠTEVKO M, SEJKORA J, DOLNÍČEK Z, ŠKÁCHA P (2018) Selenium-rich Ag–Au mineralization at the Kremnica Au–Ag epithermal deposit, Slovak Republic. *Minerals* 8: 572
- ŠTOHL J, LEXA J, KALIČIAK M, BACSÓ Z (1993) Metallogenesis of base metal stockwork mineralization in Western Carpathian Neogene volcanic rocks. Unpublished report, Geological Survey of Slovak Republic, Bratislava: 1–87 (in Slovak)
- ŠUCHA V, RODOŇ J, ZATKALÍKOVÁ V, FRANČL J (1991) Mixed layer mineral of illite/smectite type: separation, identification, use. *Miner Slov* 23: 267–274 (in Slovak with English abstract)
- ŠUCHA V, KRAUS I, GERTHOFFEROVÁ H, PETEŠ J, SEREKOVÁ M (1993) Smectite to illite conversion in bentonites and shales of the East Slovak Basin. *Clay Miner* 28: 243–253
- ŠRODOŇ J (1981) X-ray identification of randomly interstratified illite/smectite in mixture with discrete illite. *Clay Miner* 16: 297–304
- ŠRODOŇ J, DRITS VA, MCCARTY DK, HSIEH JCC, EBERL DD (2001) Quantitative X-ray diffraction analysis of clay-bearing rocks from random preparations. *Clays Clay Miner* 49: 514–528
- VALKOVIC V (1983) *Trace elements in coal*. CRC Press, Boca Raton, Florida, v 1, pp 1–304
- VLASÁČ J, CHOVAN M, VOJTKO R, ŽITŇAN P, MIKUŠ T (2021a) Mineralogy of the Au–Ag mineralization from the Finsterort and Anton vein system, Štiavnické vrchy Mts. (Slovakia). *Bull Mineral Petrolog* 29: 255–269
- VLASÁČ J, MIKUŠ T, ONDREJKA M, ŽITŇAN P, TUČEK P (2021b) Supergene Pb–Cu–(Sb) mineral assemblage in abandoned epithermal deposit Rudno nad Hronom, Slovakia. *Acta Geol Slov* 13: 107–118
- WAKETA H, SCHMIDT RA (1978) Cadmium. In: WEDEPOHL KH (ed) *Handbook of Geochemistry*, vol. II-4. Springer-Verlag Berlin
- WANG L, QIN K-Z, SONG G-X, LI G-M (2019) A review of intermediate sulfidation epithermal deposits and subclassification. *Ore Geol Rev* 107: 434–456
- WEDEPOHL KH (1995) The composition of the continental crust. *Geochim Cosmochim Acta* 59: 1217–1232
- WU D (1987) Phase relations in the system  $Ag_2S$ – $Cu_2S$ – $PbS$  and  $Ag_2S$ – $Cu_2S$ – $Bi_2S_3$  and their mineral assemblages. *Chin J Geochem* 6: 225–233